Cell Reports

Article

Regulation of ERK2 activity by dynamic *S*-acylation

Graphical abstract

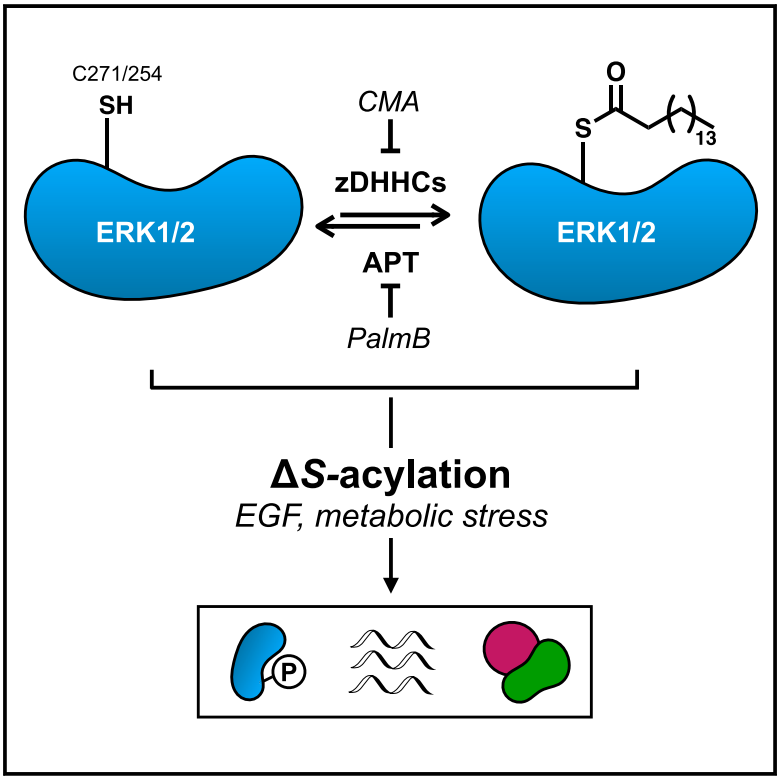

Highlights

- *S*-acylation of ERK1/2 occurs at C271/C254 and responds to EGF stimulation
- Perturbation of *S*-acylation alters ERK2 activation and transcriptional program
- A panel of DHHC-family proteins increases ERK1/2 *S*-acylation
- ERK1/2 *S*-acylation is altered in a mouse model of metabolic disease

Authors

Saara-Anne Azizi, Tian Qiu, Noah E. Brookes, Bryan C. Dickinson

Correspondence

dickinson@uchicago.edu

In brief

Azizi et al. introduce *S*-acylation as an EGF-responsive post-translational modification of ERK1/2. Further studies highlight its impact on ERK2 activation and the consequences for downstream signaling. Moreover, a mouse model of metabolic disease reveals organ-specific changes in the levels of ERK1/2 *S*-acylation.

Azizi et al., 2023, Cell Reports *42*, 113135
September 26, 2023
https://doi.org/10.1016/j.celrep.2023.113135

CellPress

Cell Reports

CellPress
OPEN ACCESS

Article

Regulation of ERK2 activity by dynamic *S*-acylation

Saara-Anne Azizi,[1,2] Tian Qiu,[1] Noah E. Brookes,[1] and Bryan C. Dickinson[1,3,*]
[1]Department of Chemistry, The University of Chicago, Chicago, IL 60637, USA
[2]Medical Scientist Training Program, Pritzker School of Medicine, The University of Chicago, Chicago, IL 60637, USA
[3]Lead contact
*Correspondence: dickinson@uchicago.edu
https://doi.org/10.1016/j.celrep.2023.113135

SUMMARY

Extracellular signal-regulated kinases (ERK1/2) are key effector proteins of the mitogen-activated protein kinase pathway, choreographing essential processes of cellular physiology. Here, we discover that ERK1/2 are subject to *S*-acylation, a reversible lipid modification of cysteine residues, at C271/C254. The levels of ERK1/2 *S*-acylation are modulated by epidermal growth factor (EGF) signaling, mirroring its phosphorylation dynamics, and acylation-deficient ERK2 displays altered phosphorylation patterns. We show that ERK1/2 *S*-acylation is mediated by "writer" protein acyl transferases (PATs) and "eraser" acyl protein thioesterases (APTs) and that chemical inhibition of either lipid addition or removal alters ERK1/2's EGF-triggered transcriptional program. Finally, in a mouse model of metabolic syndrome, we find that ERK1/2 lipidation levels correlate with alterations in ERK1/2 lipidation writer/eraser expression, solidifying a link between ERK1/2 activity, ERK1/2 lipidation, and organismal health. This study describes how lipidation regulates ERK1/2 and offers insight into the role of dynamic *S*-acylation in cell signaling more broadly.

INTRODUCTION

Protein *S*-acylation, the addition of a long-chain fatty acid to a cysteine residue via a thioester bond, is a lipid post-translational modification (PTM) known to affect the activity and function of modified proteins. Protein *S*-acylation dynamics are enzymatically mediated, with DHHC (Asp-His-His-Cys) domain-containing protein acyl transferases (PATs) acting as "writers" and acyl protein thioesterases (APTs) as "erasers."[1] At the cellular level, these cycles of *S*-acylation and deacylation regulate protein subcellular trafficking and activity, and at the organismal level, have been implicated in cancer and neurological and inflammatory disease.[2] One area in which the role of *S*-acylation has been increasingly recognized is signal transduction, with receptors (MC1R, EGFR) and effectors (AKT, JNK, STAT3) requiring *S*-acylation for activity and downstream functionality.[3–7] However, while the advent of chemical and biochemical techniques to study protein lipidation has precipitously increased our knowledge of the frequency and significance of *S*-acylation, the consequences of dynamic *S*-acylation for many proteins remain unknown.

Mitogen-activated kinases (MAPKs) are an evolutionarily conserved family of proteins that are critical in transducing extracellular signals to the interior of the cell and in regulating a diverse array of cellular programs.[8,9] Particularly well studied in this venerable family are extracellular signal-regulated kinases (ERK1/2). As the primary mediators of the Ras cascade, ERK1/2 phosphorylate hundreds of cytoplasmic and nuclear substrates, regulating processes such as embryogenesis, cell motility, proliferation, differentiation, and apoptosis.[10–12] ERK1/2-dependent signal transduction is also critical in cellular and organismal metabolism, contributing to glycolytic pathway reprogramming (Warburg effect) in normal and cancer cells and to development of metabolic syndrome.[13]

The simple architecture of the central three-tiered cascade belies its complexity and finely tuned ability to determine specific cell responses. In fact, the master regulators ERK1/2 are themselves intricately regulated. Subcellular localization, docking motif-mediated interactions with substrates and regulatory elements, scaffolding proteins, phosphatases, and crosstalk with other signaling pathways all modulate ERK specificity and activity.[14–16] Central to the ERK1/2 regulatory scheme are PTMs, in particular phosphorylation. MEK1/2-mediated dual phosphorylation of a threonine-glutamic acid-tyrosine (TEY) motif is critical in regulating ERK1/2 activity following upstream signaling events. The magnitude and duration of phosphorylation at this motif determines the specific ERK1/2 transcriptional program. Other serine and threonine residues in ERK1/2 are also phosphorylated and regulate ERK1/2 activity.[17–19] More recently, other PTMs have emerged as negative regulators of ERK1/2 activity, including *S*-nitrosylation of Cys183, acetylation of Lys72, and tri-methylation of Lys302/361 of ERK1.[20–22]

Despite its extensiveness, the established network of regulatory mechanisms does not fully explain how activation of ERK1/2 by multiple extracellular stimuli results in distinct cellular outcomes, suggesting that there is still more to be discovered about the regulation of ERK1/2 activity and function.[23–26] Intriguingly, proteomics studies suggest that ERK1/2 might be subject to *S*-acylation,[27] leading us to hypothesize that lipidation may contribute to ERK1/2 regulation. Here, we show that ERK1/2 is *S*-acylated, in particular *S*-palmitoylated, *in cellulo* and *in vivo*. Moreover, we establish that ERK1/2 *S*-acylation levels are

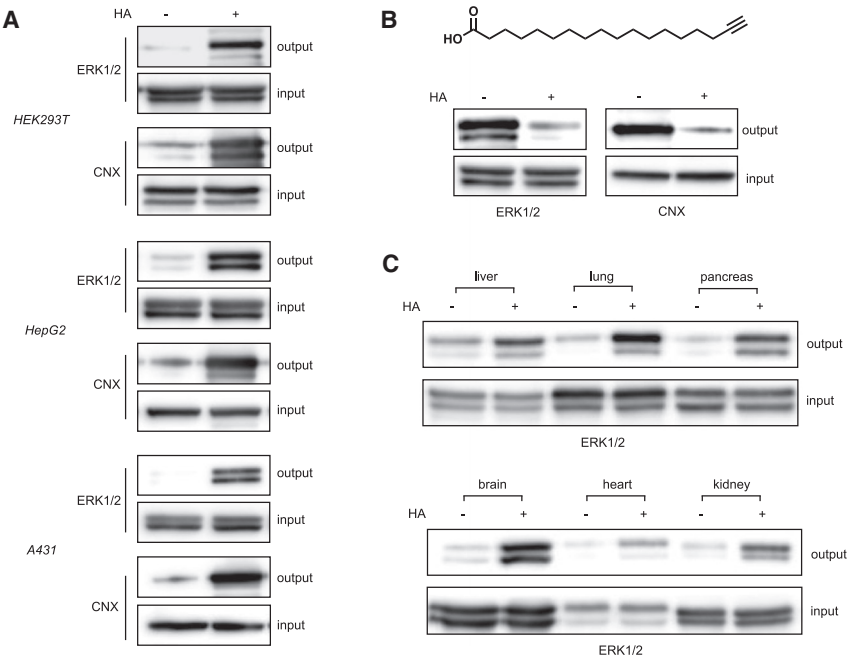

Figure 1. ERK1/2 are *S*-palmitoylated

(A) Acyl biotin exchange (ABE) assay carried out in HEK293T, HepG2, and A431 cells, where signal in hydroxylamine (HA)-treated samples indicates *S*-acylation. Calnexin (CNX) is used as a loading and assay control. n = 3.

(B) Metabolic labeling with 17-octadecynoic acid (17-ODYA) in HEK293T cells. Signal in the "−HA" lanes indicates incorporation of the 16C fatty acid, while loss of signal in the "+HA" samples indicates thioester bond formation. n = 2.

(C) ABE carried out on a panel of tissues harvested from C57BL/6 mice to visualize *S*-acylation *in vivo*.

dynamically regulated during epidermal growth factor (EGF) stimulation and that *S*-acylation regulates the pattern of its TEY and serine phosphorylation, its protein interaction partners, and subsequent activation. We then show that ERK1/2 *S*-acylation is enzymatically mediated by dynamic associations with a subset of DHHC-PATs, which install the acyl group, and identify APT2 as a candidate eraser of the acyl group. Finally, we use a mouse model of metabolic syndrome to profile changes in *S*-acylation correlated with aberrant activity and changes in writer and eraser protein expression. This work introduces *S*-acylation as a regulatory module of ERK1/2 activity and potential therapeutic node for targeting ERK1/2 activity not only in metabolic syndrome but in cancer and other MAPK signaling-driven pathologies.

RESULTS

ERK1/2 *S*-acylation levels respond to EGF stimulation

ERK1/2 acylation has been hinted by thiopropyl capture experiments carried out in adipocytes.[27] Therefore, we sought to confirm that *S*-acylation, and more specifically, *S*-palmitoylation, is a PTM of ERK1/2. To visualize cysteine acylation, we first used acyl biotin exchange (ABE), in which the labile thioester bond of acylated cysteine is cleaved by hydroxylamine (HA) and substituted with an enrichment handle.[28] This assay, which was carried out in HEK293T, A431, and HepG2 cells, revealed that ERK1/2 are *S*-acylated across cell lines (Figures 1A and S1A). Next, to corroborate these results and confirm the incorporation of palmitate, we used metabolic labeling with 17-octadecynoic acid (17-ODYA), the ω-alkyne analog of 16C palmitic acid (Figure S1A). Here, we observed incorporation of the tagged palmitic acid in HEK293T cells, affirming ERK1/2 *S*-palmitoylation (Figure 1B).[29] Importantly, HA treatment diminished the signal in this experiment, confirming thioester bond formation and, thus, cysteine modification (Figure 1B). We also probed ERK *S*-acylation by ABE in mouse tissues, observing significant *S*-acylation across all tissues profiled, especially in the brain, liver, and pancreas, confirming ERK *S*-acylation *in vivo* (Figure 1C). Together, these results establish that ERK1/2 are *S*-acylated at the cellular and organismal levels.

Central to ERK1/2's mediation of cellular events is their ligand-induced activation, which stimulates a rapid increase in their phosphorylation and then downstream kinase activity. We next sought to determine whether the levels of ERK1/2 *S*-acylation are sensitive to ligand-induced activation; changes in ERK1/2 *S*-acylation concurrent with activity changes could hint at a regulatory role of *S*-acylation in ERK1/2 activation. We therefore monitored ERK1/2 *S*-acylation levels upon stimulation with EGF, a secreted peptide that activates a signal transduction network that includes the RAS/ERK pathway.[25] Upon treatment of serum-starved cells with EGF, basal *S*-acylation of ERK1/2 increases within 5 min and remains elevated through 15 min of stimulation, with a return to baseline acylation levels occurring by 30 min in HepG2 and A431 cells (Figures 2A, S1B, and S1C). Significantly, this pattern mirrors that of ERK phosphorylation, which also remains elevated through 15 min and decreases by 30 min.[30] Because much remains unknown about how the extracellular concentration of ligand (signal strength) is relayed intracellularly, we next assessed the dose dependence of ERK1/2's *S*-acylation increase. As EGF concentration increased from 0 to 1 to 10 ng mL^{-1}, ERK1/2 *S*-acylation increased in step, with a lessening increase at 100 ng mL^{-1} in HepG2 and A431 cells. This suggests that *S*-acylation is responsive to the flow of quantitative information through the pathway (Figures 2B, S1D, and S1E). These results established our activating concentration of EGF at 1 ng mL^{-1}, a concentration congruent with reported physiologic levels of the growth factor in some tissues.[31] Finally, to assess the generality of the ERK *S*-acylation dynamics, we probed for ERK1/2 *S*-acylation changes upon treatment with insulin, another signaling ligand also established to activate the ERK/MAPK pathway. To our surprise, insulin treatment did not trigger an increase in ERK1/2 *S*-acylation in HepG2 or A431 cells, although a decrease in *S*-acylation was observed in A431 cells at 30 min (Figures 2C and S1F).

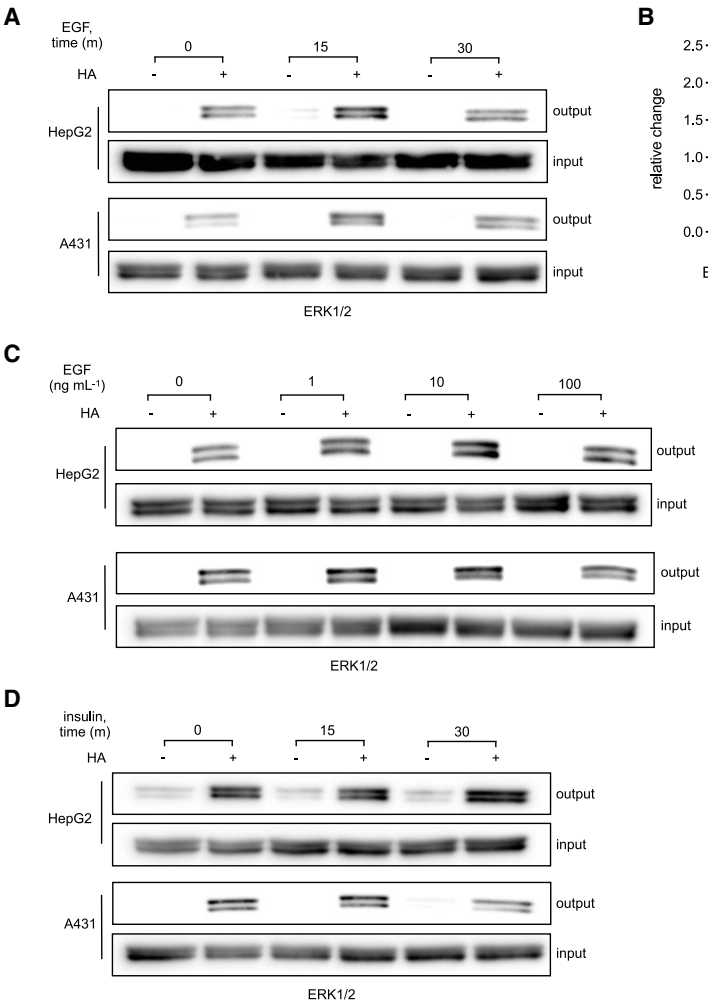

Figure 2. ERK1/2 *S*-acylation responds to EGF stimulation

(A) ABE assay carried out in HepG2 and A431 cells following stimulation with EGF (1 ng mL^{-1}) for 0, 15, and 30 min. n = 6.

(B) Quantification of (A), showing the relative fold change in ERK1/2 *S*-acylation after stimulation with EGF (1 ng mL^{-1}) at t = 15 min relative to t = 0. Statistical analysis was performed with a two-tailed Student's t test with equal variance; $p < 0.05$.

(C) ABE assay carried out in HepG2 and A431 cells following stimulation with 0, 1, 10, and 100 ng mL^{-1} EGF for 15 min. n = 3.

(D) ABE assay carried out in HepG2 and A431 cells following stimulation with insulin for 0, 15, and 30 min. n = 3.

Thus, *S*-acylation of ERK1/2 is not only dynamic but also sensitive to signal strength and signal identity, emphasizing its potential as a regulator of ERK1/2 activity.

Dynamic ERK *S*-acylation does not depend on TEY motif phosphorylation

Given that the timing of ERK1/2's dynamic *S*-acylation corresponds to that of its dynamic TEY phosphorylation, we next attempted to parse the connection between the two modifications. First, we used ABE to determine the *S*-acylation status of active ERK1/2; i.e., ERK1/2 that have been phosphorylated at the TEY motif of their activation loops. Here, we observed palmitoylated ERK1/2 increasing concomitant with ERK1/2 phosphorylation (Figure 3A). This result confirms that the two PTMs can co-occur on ERK1/2. We next used established MAPK pathway inhibitors to investigate whether the signaling elements that regulate phosphorylation also regulate ERK1/2's dynamic palmitoylation. Pre-treatment with upstream inhibitors for MEK (AZD6244, CI-1040) and RAF (PLX-4720) as well as with okadaic acid, an inhibitor of ERK1/2-directed phosphatase activity, inhibited the EGF-induced increase in ERK1/2 *S*-acylation (Figures S2A and S2B).[32–35] These results suggest that intact regulatory infrastructure is necessary for dynamic S-acylation of ERK1/2. However, while these data establish that dynamic *S*-acylation of ERK1/2 is connected to pathway activation, they do not reveal whether ERK1/2 phosphorylation itself is necessary for *S*-acylation.

To gain further insight into the sequentiality and interdependence of the two modifications, we created variants of ERK2, the more widely and abundantly expressed isoform of ERK, in which the three sites of the phospho-acceptor motif were mutated to either alanine (AAA) or glutamic acid (EEE). These mutations, respectively, confer resistance to or mimic constitutive phosphorylation, enabling us to probe the effect of perturbing ERK2 phosphorylation on its palmitoylation. Overexpression of these constructs in HEK293T cells, followed by EGF stimulation and visualization of acylated proteins, indicated that ERK2's dynamic *S*-acylation was not disrupted in either the constitutively inactive or active constructs (Figure 3B). This suggests that the EGF-mediated increase in ERK2's *S*-acylation is not dependent on its phosphorylation status. Interestingly, the levels of basal *S*-acylation in serum-starved cells increased for both constructs relative to the wild type (WT) even when accounting for expression changes, again hinting at a more complicated regulatory network (Figures 3B and S2C). Collectively, these results demonstrate that dynamic ERK1/2 *S*-acylation is dependent on pathway activation but remains intact when phosphorylation of ERK is disrupted.

Acylation-deficient ERK2 displays altered phosphorylation patterns

To determine the consequences of *S*-acylation for regulation and activation of ERK1/2, we next sought to generate palmitoylation-deficient variants of each ERK. This required mapping the *S*-acylation site(s), where we individually mutated each of the

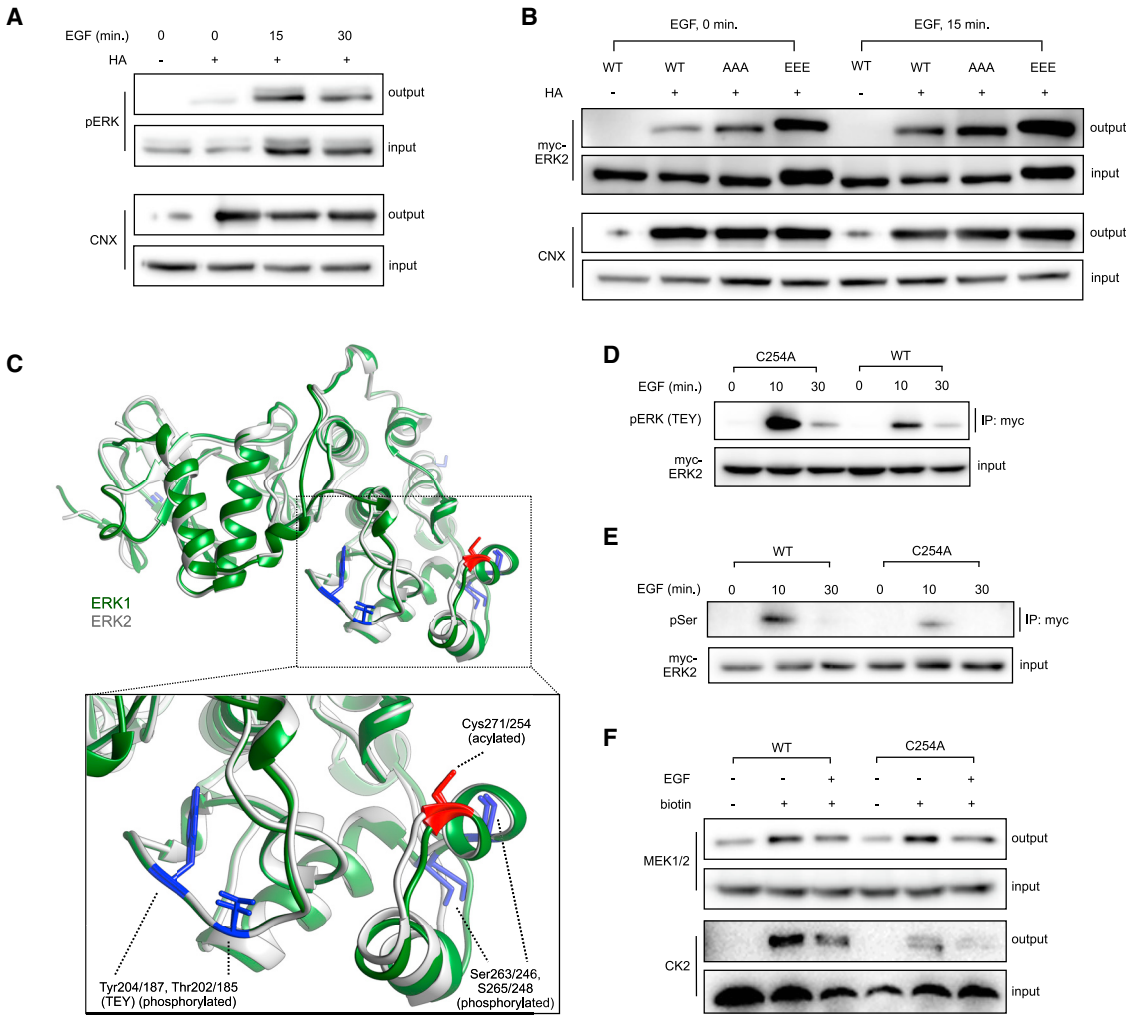

Figure 3. Mapping crosstalk between ERK2 *S*-acylation and phosphorylation

(A) ABE assay carried out in HepG2 cells and analyzed for phospho-ERK1/2 (Thr185/202, Tyr187/204) via western blotting. n = 2.

(B) ABE assay carried out in HEK293T cells overexpressing WT, TEY(AAA), or TEY(EEE) ERK2 and stimulated with EGF (1 ng mL^{-1}) for 15 min. n = 2.

(C) Crystal structure of the C-terminal lobes of ERK1 and ERK2, demonstrating structural homology as well as phosphorylation (blue) and acylation (red) sites (PDB: 6G54, 6GES).

(D) Immunoprecipitation of myc-ERK2 (WT or C254A) in HEK293T cells with or without EGF stimulation (10 and 30 min, 1 ng mL^{-1}) and analyzed via western blotting for phospho-ERK (Thr185/Tyr187). n = 3.

(E) Immunoprecipitation of myc-ERK2 (WT, C254A) with or without EGF stimulation (10, 30 min, 1 ng mL^{-1}), analyzed via western blotting for phosphoserine. n = 2.

(F) Overexpression of myc-ERK2 tagged with TurboID in HEK293T cells, followed by biotin incubation and streptavidin enrichment of labeled proteins. Enriched proteins were visualized via western blotting for MEK1/2 and CK2. n = 3.

six cysteines of ERK1 and the seven cysteines of ERK2 to serine and then used ABE to visualize the *S*-acylation status of each C-to-S mutant. For ERK1, we observed a decrease in ABE signal for C239S and C271S, and for ERK2, a decrease was seen for C216S and C254S, signifying that these cysteines are sites of *S*-acylation (Figures S3A–S3C). Because the loss of signal for C233 in ERK1 and C216 in ERK2 were accompanied by a significant loss of expression for these mutants, implicating these residues (and possibly their *S*-acylation) in the stability or proteasome degradation of ERK1/2, we chose to focus on *S*-acylation of C254 and C271. Importantly, these residues are located in the C-terminal lobe of ERK1/2, which contains their activation and catalytic loops and is also subject to other regulatory PTMs (Figure 3C).[36]

With these biochemical tools in hand, we next assessed the impact of ERK1/2 *S*-acylation on their activation, as measured by TEY phosphorylation. For this, we focused on ERK2, given that its expression exceeds that of ERK1 in most cells and that the two kinases possess highly similar sequences and identical substrate specificity *in vitro*. Overexpression of myc-tagged WT and C254A ERK2, followed by EGF stimulation and immunoprecipitation of the epitope tagged constructs, allowed visualization and comparison of TEY phosphorylation of the WT vs. *S*-acylation-deficient ERK while eliminating background signal

from endogenous ERK1/2. Strikingly, myc-ERK2(C254A) was dramatically more phosphorylated at the TEY motif than its WT counterpart (Figures 3D and S3D). This TEY hyperphosphorylation upon EGF stimulation was lost upon chemical inhibition of MEK1/2 (Figure S3E).[37] Next, because the site of *S*-acylation, C254 is most proximal not to the Thr185/Tyr187 phosphorylation sites but, rather, to the purportedly phosphorylated serine residues Ser246/248 in ERK2's putative nuclear translocation signal (NTS), we assayed for serine phosphorylation under the same conditions (Figure 3B). Here, we found that, in contrast to TEY phosphorylation, myc-ERK2(C254A) serine phosphorylation was diminished relative to that of WT ERK2 (Figure 3E). Importantly, we also found that EGF stimulation did not increase myc-ERK2(C254A) *S*-acylation, confirming that this cysteine is the site of dynamic *S*-acylation (Figure S3F). Together, these results suggest that the dynamic *S*-acylation of C254 has a substantial role in regulating the phosphorylation patterns and, we hypothesize, activation of ERK2.

Disrupting ERK2 *S*-acylation impacts regulatory interactions

It is well established that MEK1/2 mediates phosphorylation of ERK1/2's TEY motif, while CK2, a constitutively active Ser/Thr protein kinase, has been implicated as the writer of ERK2 serine phosphorylation.[38,39] Therefore, we next probed whether the observed changes in TEY and SPS phosphorylation are connected to disrupted interactions with these key regulatory partners. To do this, we generated myc-ERK2 tagged with TurboID, a biotin ligase that generates biotin-AMP to rapidly label proximal proteins and enable the mapping of the protein-protein interactions.[40] After validating the expression and ligase activity of the constructs, we used the TurboID-tagged myc-ERK2 to visualize changes in ERK2's interactions (Figure S3G). Here, we found that, while the interaction with MEK1/2 was unchanged between the WT and C254A myc-ERK2, acylation-deficient ERK2 demonstrated decreased labeling of CK2 (Figure 3F). This corresponds with the observed decrease in serine phosphorylation and suggests that C254 *S*-acylation has a role in coordinating the CK2-ERK2 interaction.

It has additionally been postulated that serine phosphorylation promotes ERK2 interactions with the nuclear transport receptor (NTR) importin 7 and contributes to its nuclear translocation.[39] Intriguingly, importin 7 is also a lipid-binding protein, and an ERK NTS-derived myristoylated phosphomimetic peptide has been shown to inhibit the ERK2-importin 7 interaction.[41,42] Therefore, we next used the TurboID constructs to visualize the acylation dependence of the ERK2-importin 7 interaction. Here, we found that impairment of ERK2 C254 *S*-acylation resulted in a diminished interaction with importin 7 (Figure S3H). While this could result from decreased serine phosphorylation, it also raises the possibility that ERK2 *S*-acylation is part of a two-step coincidence detection motif in this protein-protein interaction (Figure S3I).

Chemical inhibition of ERK1/2 *S*-acylation disrupts its transcriptional program

Upon EGF stimulation and translocation to the nucleus, ERK signaling elicits a gene expression program linked to diverse cellular events, such as proliferation and differentiation. Given the changes in phosphorylation and the possible interruption of nuclear localization, we next aimed to determine how loss of dynamic ERK1/2 *S*-acylation affects this transcriptional program. To do this, we began by identifying chemical tools to disrupt the cycle of ERK1/2 *S*-acylation and deacylation because overexpressed proteins have the potential to overload biological pathways.[43] First, we targeted installation of the lipid by DHHC-PATs using 2-bromopalmitate (2BP), a widely used albeit promiscuous inhibitor, and cyano-myracrylamide (CMA), another small inhibitor with a different reactivity profile recently developed by our group (Figure S4A).[44–46] ABE revealed that treatment with 2BP (20 μM, 6 h) failed to decrease *S*-acylation of ERK, possibly because of its poor potency and/or poor targeting of ERK-specific writers (Figure 4A). However, treatment with CMA, but not its inactive analog, under parallel conditions (20 μM, 6 h) resulted in a significant decrease of *S*-acylation of ERK1/2, with maximum inhibition of *S*-acylation reached after 3 h of treatment in HepG2 cells (Figures 4A and S4A–S4C). These results validate CMA as a tool to analyze the downstream consequences of inhibiting ERK1/2 *S*-acylation and confirm that *S*-acylation of ERK1/2 is enzymatically regulated.

Next, we used palmostatin B (PalmB), a pan inhibitor of APTs, to interrupt enzymatic lipid removal and therefore increase *S*-acylation of ERK1/2.[47] Treatment of HepG2 cells with PalmB (20 μM, 6 h) and visualization of acylated proteins via ABE showed increased ERK1/2 *S*-acylation, confirming the utility of this inhibitor in probing the effects of perturbing ERK1/2 *S*-acylation (Figures 4B and 4C). The effectiveness of PalmB also confirmed that ERK1/2 deacylation is enzymatically mediated. We next sought to determine which APT(s) are responsible for deacylation of ERK1/2. While the β-lactone PalmB acts globally on APTs, ML-348 and ML-349 are inhibitors specific for two of the most widely studied *S*-deacylases, APT1 and APT2, respectively.[48,49] We found that a slight increase in ERK *S*-acylation only occurred with ML-349 treatment, suggesting that APT2, but not APT1, potentially regulates deacylation of ERK1/2 (Figure S4D). However, because the increase was less than that observed with PalmB, it also introduces the possibility that additional APTs have a role in regulation of ERK1/2 and establishes PalmB as the key tool to disrupt ERK1/2's deacylation.

With these validated chemical inhibitors of ERK1/2 *S*-acylation and deacylation in hand, we next aimed to assess the consequences of disrupted *S*-acylation for ERK1/2 transcriptional regulation. As the key activators of MAPK pathway, ERK1/2 are connected to induction of hundreds of gene targets, including cFos, early growth response proteins 1/2 (EGR1/2), and dual-specificity phosphatases 1/6 (DUSP1/6).[50] Quantitative reverse-transcription PCR (qRT-PCR), following pretreatment of HepG2 cells with DMSO, CMA, or PalmB and stimulation with EGF (0, 30, and 60 min), revealed inhibitor-dependent changes in the induction pattern of these genes (Figures 4D and S4E). In the case of the immediate-early response genes cFos and EGR1/2, treatment with CMA and PalmB limited the rapid mRNA transcription typically observed after 30 min of EGF treatment compared with the DMSO control. However, after 60 min, cFos and EGR1 transcript levels matched the control sample, while EGR2 transcript levels continued to rise. This

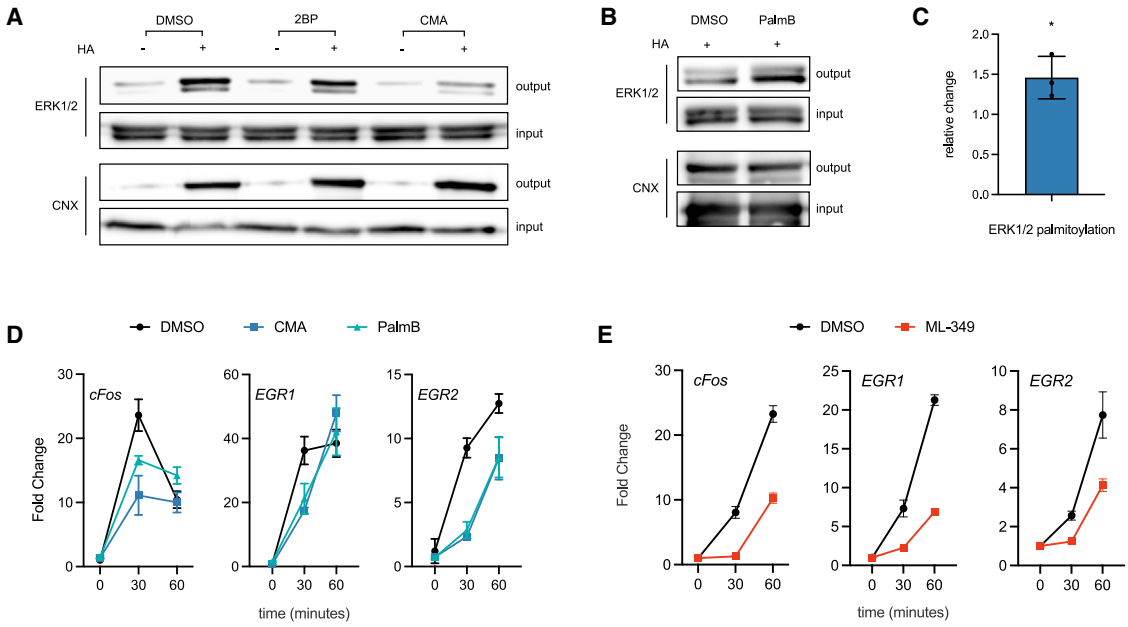

Figure 4. Chemical perturbation of ERK1/2 *S*-acylation disrupts their transcriptional program

(A) ABE assay carried out in HepG2 cells treated with DMSO, 2BP (20 μM), or CMA (20 μM) for 6 h. CNX is used as a loading and assay control. n = 3.

(B) ABE assay carried out in HepG2 cells treated with DMSO or PalmB (20 μM) for 6 h. CNX is used as a loading and assay control. n = 3.

(C) Quantification of (B), showing the relative fold change in ERK1/2 *S*-acylation after treatment with PalmB. Statistical analysis was performed with a two-tailed Student's t test with equal variance; $p < 0.05$.

(D) qRT-PCR of key transcripts in the EGF-stimulated transcriptional program in HepG2 cells treated with DMSO, CMA (20 μM), or PalmB (20 μM) for 3 h, followed by stimulation with EGF (1 ng mL^{-1}) for 0, 30, and 60 min. n = 3.

(E) qRT-PCR of key transcripts in the EGF-stimulated transcriptional program in HepG2 cells treated with DMSO or ML-349 (20 μM) for 3 h, followed by stimulation with EGF (1 ng mL^{-1}) for 0, 30, and 60 min. n = 3.

suggests that disruption of ERK1/2 *S*-acylation—its installation and removal—delays rather than inhibits its EGF-stimulated transcriptional program. For the immediate-late gene DUSP1, PalmB treatment resulted in increased activation at 60 min, while DUSP6 expression was dampened at all time points. Notably, treatment with the APT2 inhibitor ML-349 paralleled the effects of PalmB on key targets in the transcriptional program, supporting its claim as a regulator of ERK2 *S*-acylation (Figure 4E). The importance of *S*-acylation in regulating the transcriptional program was further substantiated by studies with WT and acylation-deficient ERK2. Overexpression of these two constructs, followed by stimulation with EGF and qRT-PCR for key transcripts, revealed a pattern of delayed activation as well, albeit with amplitude changes likely reflecting background activation from overexpression (Figure S4F). Together, these alterations suggest that the cycle of *S*-acylation is significant for regulating the timing and amplitude of ERK-mediated gene expression changes.

ERK2 *S*-acylation is mediated by dynamic associations with DHHCs and APTs

Having determined that dynamic *S*-acylation is significant for ERK1/2 activity, we next sought to identify the molecular determinants of this PTM. Identification of these regulatory elements (i.e., the writers and erasers) could enable more controlled modulation ERK *S*-acylation and therefore represents a potentially novel way to manipulate ERK1/2 activity. Typically, the "Fukata assay," overexpression of 23 mammalian zDHHCs,[51] followed by visualization of *S*-acylation via ABE, is used to ascertain the DHHC-PAT writers of a particular substrate. However, in this screen, while slight increases in ERK1/2 *S*-acylation were observed with overexpression of some zDHHCs, no definitive writers for ERK1/2 were identified (Figure S5A). This could suggest that ERK1/2 *S*-acylation is regulated by multiple PATs, with compensatory down-regulation complicating observation of increases in *S*-acylation. In addition, the levels of ERK1/2 *S*-acylation are likely tightly regulated, and the ABE assay reveals the steady-state levels of *S*-acylation for a target, not the cycling of *S*-acylation mediated in part by the PATs. Therefore, we next used metabolic labeling to visualize a change in the rate of *S*-acylation via increased incorporation of an alkyne-tagged fatty acid. Here, we observed that a panel of PATs (annotated as zDHHC 2, 3, 7, 9, 11, 23, 12, 14, 15, 17, 20, 21, and 25) increased ERK1/2 palmitoylation, with zDHHCs 7, 11, 14, 15, 20, 21, and 25 being the strongest hits for ERK1 and ERK2 (Figures 5A and S5B). Because we had observed two sites of *S*-acylation for ERK2 (C216 and C254), we also used the metabolic labeling-coupled DHHC overexpression assay with the ERK2(C254A) mutant to assess the site specificity of these writers (Figures 5A and S5C). Here, we found that, while a portion of the PATs (11, 12, 15, 20, 21, and 25) that increased palmitoylation of ERK1/2 also increased

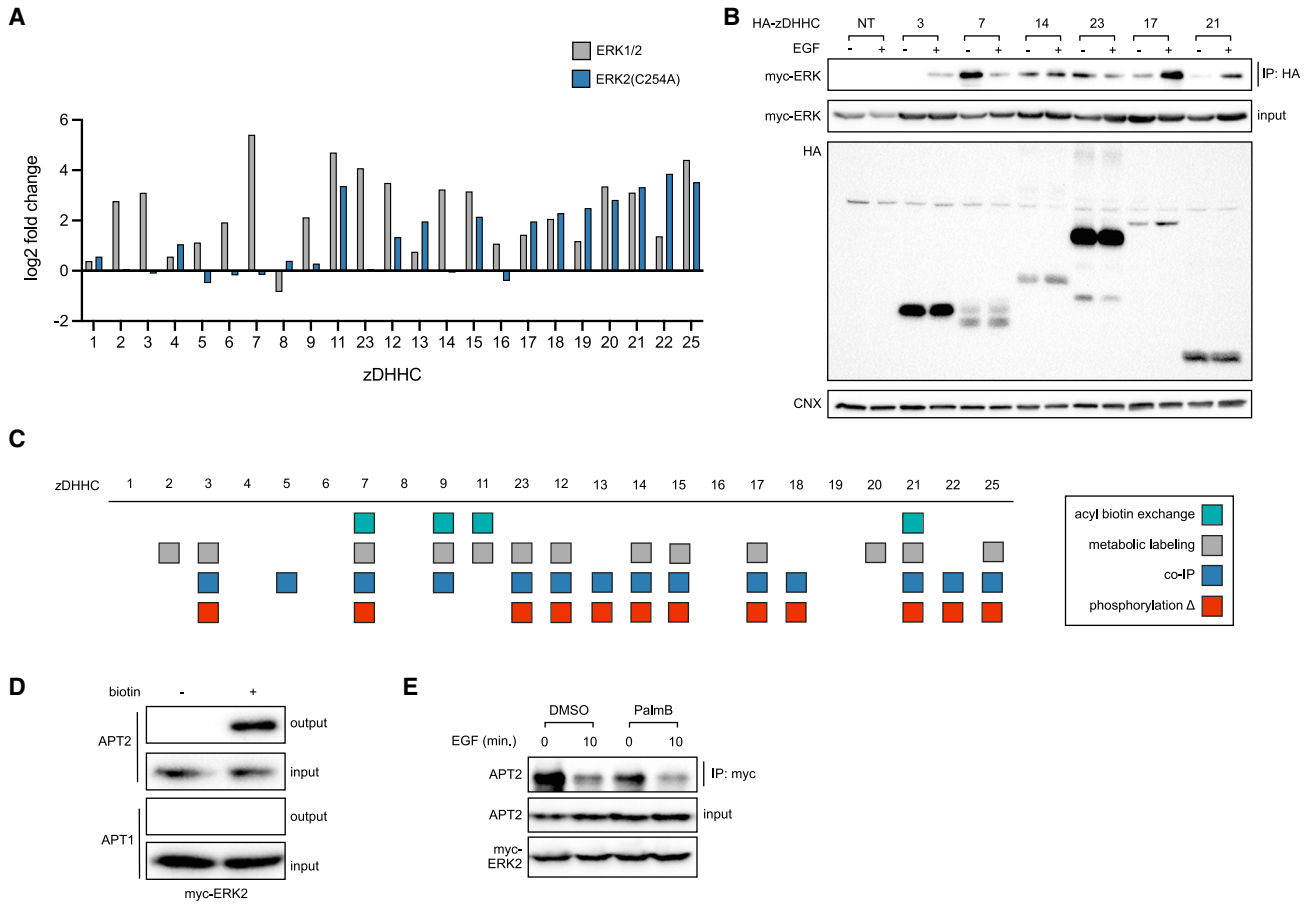

Figure 5. ERK2's acylation is mediated by dynamic associations with writer and eraser proteins

(A) Quantification of ERK1/2 metabolic labeling with 17-ODYA (relative to an NT control) in HEK293T cells overexpressing murine DHHC-family proteins with and without myc-ERK2(C254A). n = 2.

(B) Immunoprecipitation using an anti-HA antibody in HEK293T cells expressing the indicated HA-tagged DHHC protein with or without EGF stimulation (10 min, 1 ng mL^{-1}). Co-immunoprecipitated proteins were visualized via western blotting for myc-ERK2. n = 2.

(C) Diagram summarizing the DHHC "hits" from the four assays (ABE, metabolic labeling, TEY phosphorylation changes, and co-immunoprecipitation) used to ascertain ERK2 writers.

(D) Overexpression of myc-ERK2 tagged with TurboID in HEK293T cells, followed by biotin incubation and streptavidin enrichment of labeled proteins. Enriched proteins were visualized via Western blotting for APT1 and APT2. n = 3.

(E) Co-immunoprecipitation of APT2 with myc-ERK2 in HEK293T cells with or without EGF stimulation (10 min, 1 ng mL^{-1}) and with or without PalmB treatment (20 μM, 3 h). Co-immunoprecipitated proteins were visualized via western blotting for APT2. n = 3.

palmitoylation of ERK2(C254A), certain PATs (namely, zDHHCs 13, 19, and 22) were writers of ERK2(C254A) and, thus, C216 only (Figures S5B and S5C). This suggests that the remaining identified PATs (zDHHC 2, 3, 7, 9, 23, and 14) possess specificity for C254.

Given that metabolic labeling implicated a large number (13/23) of DHHC proteins as ERK1/2 writers, we next aimed to determine which were significant in its EGF-promoted dynamic *S*-acylation. Having observed a change in TEY phosphorylation of palmitoylation-deficient ERK2, we next probed for changes in ERK2 EGF-stimulated TEY phosphorylation concurrent with DHHC overexpression. In this screen, we observed that a number of DHHCs (3, 7, 23, 12, 13, 14, 15, 17, 18, 21, 22, and 25) increased ERK2 TEY phosphorylation, with strong overlap (7/12) with writers identified via metabolic labeling (Figures 5C and S5D). For final validation, we also assessed the physical writer/substrate interaction in the context of EGF signaling via co-immunoprecipitation of ERK2 by HA-tagged zDHHC-family proteins. Here, a panel of DHHCs (3, 5, 7, 9, 11, 14, 17, 18, 20, 21, 22, and 23) interacted with ERK2 (Figures 5B, 5C, and S5E). Summation of the results confirmed DHHC 7 and 21–hits in all assays and thought to be localized to the Golgi apparatus and plasma membrane, respectively–as key writers of ERK2 *S*-acylation.[52] Significantly, ERK2 association with certain PATs was dynamic, with ERK2 dissociating from zDHHCs 5, 7, and 23 and associating with zDHHCs 3, 17, and 21 upon stimulation with EGF (Figure S5E). These results demonstrate that certain DHHC family members are not just writers of ERK2 *S*-acylation, they are also central to its dynamic *S*-acylation during EGF signaling.

The other vital element in the cycle of *S*-acylation/deacylation are the erasers, the APTs.[53–55] To identify candidate erasers, we first overexpressed the cytosolic serine hydrolases annotated as APTs, APT1, APT2, and ABHD17 A/B/C, and assayed for resultant changes in ERK1/2 *S*-acylation. Here, no discernible decreases, which would indicate ERK1/2-targeted eraser activity, were observed (Figure S5F). We also found no observable change in *S*-acylation of ERK2(C254A) with overexpression of known APTs (Figure S5G). Because previous experiments with the inhibitor ML-349 intimated that APT2 was a candidate eraser, we next decided to see whether knockdown of this protein (encoded by LYPLA2) would elicit a change in ERK1/2 *S*-acylation. However, small interfering RNA (siRNA)-mediated knockdown of APT2 or APT1/2 together did not increase ERK1/2 *S*-acylation; in fact, a decrease was observed (Figure S5H). These results again suggest that steady-state level *S*-acylation of ERK2 is tightly regulated.

Given the challenges of identifying the eraser via observations of steady-state ERK1/2 *S*-acylation, we used our TurboID-tagged myc-ERK2 to map the interactions of ERK2 with APT1 and 2. Here, we observed labeling of and, thus, proximity to APT2 but not APT1 (Figure 5D). This labeling of APT2 but not APT1 was also observed with ERK2(C254A), suggesting, not unexpectedly, that the APT2-ERK2 interaction requires more than lipid recognition (Figures 5D and S5I). To confirm this observation and establish the relevance of APT2 in ERK2's dynamic *S*-acylation, we next carried out co-immunoprecipitation of APT2 with myc-ERK2 with and without EGF stimulus. This revealed a decrease in the interaction between ERK2 and APT2 upon addition of EGF, an interaction that was also diminished upon treatment with PalmB (Figure 5E). In total, these observations further substantiate a model of dynamic ERK *S*-acylation, modulated by the interplay of several DHHCs and APT2, in regulation of its EGF-induced activity.

ERK1/2 *S*-acylation is altered under conditions of metabolic stress

ERK1/2 signaling is not only responsive to growth factors but also to cellular metabolism, with diet-derived molecules, such as glucose and long-chain fatty acids, influencing enzyme activity and gene expression.[56] In fact, dysregulated ERK signaling, resulting from aberrant nutrient levels, has been implicated in the pathogenesis of metabolic syndrome.[57] While the mechanisms of this phenomenon are unknown, metabolite-dependent PTMs, such as *S*-acylation, present an intuitive, albeit unestablished, regulatory mechanism.[58] Thus, we aimed to determine whether changes in *S*-acylation of ERK1/2 could contribute to the changes in its activity *in cellulo* and *in vivo.* Incubation of HepG2 cells with a bolus of palmitate (500 μM), a condition known to induce metabolic stress and alter ERK1/2 activation, decreased ERK1/2 *S*-acylation levels, confirming the sensitivity of ERK1/2 *S*-acylation to metabolic stressors (Figures 6A and S6A).

We next assessed changes in ERK1/2 *S*-acylation in relevant tissues in a mouse model of diet-induced obesity. C57BL/6J were fed either a high-fat diet (HFD) rich in palmitate or a matched control diet (CD) for 18 weeks and then evaluated for metabolic health (Figures 6B, 6C, and S6B).[59] After confirming the onset of metabolic syndrome in HFD mice, we probed for changes in ERK1/2 *S*-acylation in the liver, a metabolically active tissue in which ERK signaling is dysregulated in obesity, and the brain, a tissue with known sensitivity to circulating palmitate levels.[60–62] Here, we observed an increase in *S*-acylation of ERK1/2, especially for ERK2, in the liver, while a decrease was observed in the brain (Figures 6D and 6E). Interestingly, the MAPK pathway signaling response to metabolic imbalance is not thought to be congruent across tissues; hepatic ERK overactivation is a known contributor to insulin resistance, while sustained ERK1/2 signaling in the hypothalamus promotes normoglycemia.[57,63–65] Thus, our observation of opposite changes in ERK1/2 *S*-acylation levels in the liver and brain in fact corresponds with reported changes in activity and lends credence to a mechanism that links elevated metabolite levels, *S*-acylation, and dysregulated signaling. Moreover, transcript abundance estimation via qRT-PCR indicated corresponding changes in the expression of ERK2 writers, with DHHCs 9, 14, and 17 and APT2 downregulated in the liver and DHHCs 3, 7, 9, 14, 17, 21, and 23 downregulated in the brain (Figures 6F–6I). Intriguingly, the decrease in APT expression in the liver paralleled the increase in ERK *S*-acylation, while the decrease in DHHC expression in the brain paralleled the decrease in ERK *S*-acylation. These results suggest that the enzyme-mediated changes in *S*-acylation of ERK1/2 could contribute to the mechanism of dysregulated ERK1/2 signaling observed across tissues in metabolic syndrome.

DISCUSSION

As members of the conserved MAPK family, ERK1/2 contribute to essential cell processes and are associated with cell proliferation, cell growth, cell mobility, and cell survival.[66] Targeting ERK1/2 activity is of therapeutic interest for a constellation of pathological conditions, including cancer, metabolic syndrome, neurological disease, and chronic inflammation.[57,67–69] Here, we introduce *S*-acylation as a signal-responsive PTM for ERK1/2, in particular ERK2. The dynamics observed (i.e., increasing *S*-acylation with EGF treatment) are in accordance with our previously reported rapid decrease in APT activity upon EGF treatment and highlight the regulatory role of this PTM and the potential of APT activity to tune substrate lipidation levels.[70–72] In addition, when coupled with the observed specificity of the increase (EGF over insulin) and the previously described role of phosphorylation in regulating APT1 activity, this suggests a so far undescribed cellular conversation between the acylation-regulatory machinery and canonical phosphorylation cascades.[73] Defining the nature of these upstream interactions represents a new and significant line of investigation.

Our experiments also highlight the relevance of *S*-acylation for ERK2 activity and function. Although mutation (activation/inactivation) of the canonical TEY motif did not disrupt the dynamics of ERK2 *S*-acylation, biochemical perturbation of a primary acylation site of ERK2, C254, resulted in an altered pattern of phosphorylation for its activation loop TEY motif and serine residues. Mutation of this site also disrupted ERK2's interactions with the kinase CK2 and the NTR importin 7. Given the observed changes in phosphorylation and regulatory interactions, which are

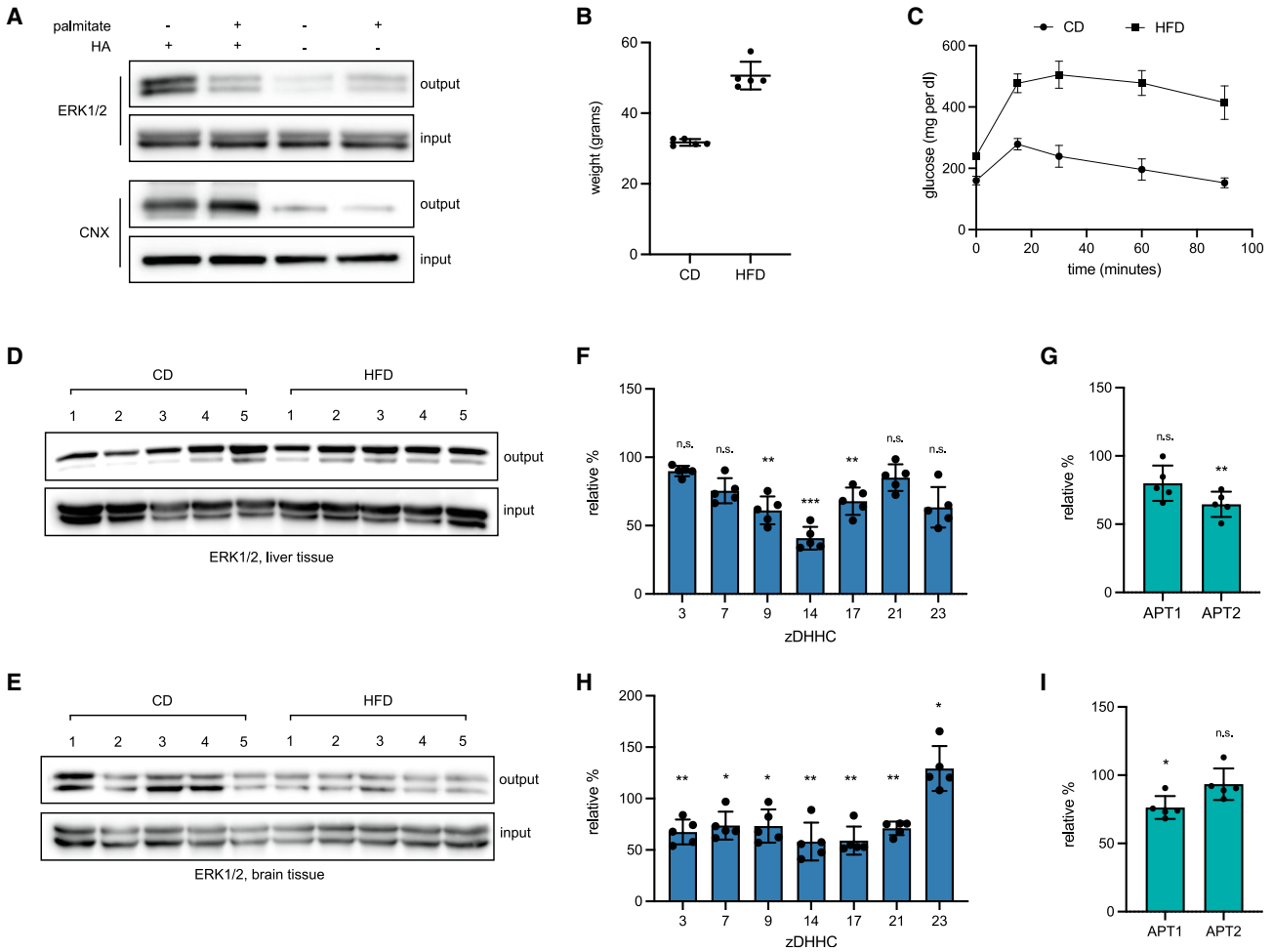

Figure 6. ERK1/2 *S*-acylation is responsive to metabolic stress *in cellulo* and *in vivo*

(A) ABE assay in HepG2 cells treated with palmitate (0 or 500 μM). n = 3.

(B) Plot of the weight of mice fed either a control diet (CD) or high-fat diet (HFD). Mean ± SD, n = 5.

(C) Glucose tolerance test (GTT) for mice fed either a CD or an HFD. Mean ± SD, n = 5.

(D) ABE assay carried out on liver tissues of C57BL/6 fed either a CD or HFD for 20 weeks.

(E) ABE assay carried out on brain tissues of C57BL/6 fed either a CD or HFD for 20 weeks.

(F) qRT-PCR analysis of ERK DHHC writer transcript levels in the liver of HFD mice relative to those of CD mice.

(G) qRT-PCR analysis of APT transcript levels in the liver of HFD mice relative to those of CD mice. Statistical analyses were performed with a two-tailed Student's t test with equal variance (n = 5). *p < 0.05, **p < 0.005, ***p < 0.0005..

(H) qRT-PCR analysis of ERK DHHC writer transcript levels in the brain of HFD mice relative to those of CD mice.

(I) qRT-PCR analysis of APT transcript levels in the brain of HFD mice relative to those of CD mice. Statistical analyses were performed with a two-tailed Student's t test with equal variance (n = 5). *p < 0.05, **p < 0.005, ***p < 0.0005.

significant for ERK2 activation and activity, we also assessed the effect of disrupting the cycle of ERK1/2 *S*-acylation on their transcriptional program. Here, we observed that chemical inhibition of lipid installation and removal disrupted the activation timing and amplitude of targets like EGR1, cFos, and DUSP6 (Figures 4C and 4D). This suggests that an inhibitor targeting C254 of ERK2, or possibly C271 of ERK1, could be used to regulate their activity and downstream cellular events. The potential of cysteine-reactive chemical tools to moderate ERK1/2 is also highlighted by the observation that the decreased expression of ERK1/2 coincident with the mutagenesis of Cys233/216 can be reversed by addition of either the proteasome inhibitor MG132 or the APT2 inhibitor ML-349, although further studies are needed to understand the intersection between *S*-acylation and ubiquitination-dependent degradation (Figure S6B). Finally, while there are currently at least three overlapping models of ERK1/2 nuclear translocation, our observations suggest that the story is not yet complete; perhaps *S*-acylation has a role to play as well. We posit that the TEY hyperphosphorylation and shifted transcriptional program timing could reflect increased ERK2 cytoplasmic time in the setting of alterations in the ERK/CK2/importin 7 interactions (Figures 3 and 4).

We additionally identified the enzymatic mediators of ERK1/2's *S*-acylation and a candidate enzyme for its deacylation,

with zDHHCs 7 and 21 emerging as two of several writers and APT2 as a possible eraser (Figure 5). Interestingly, traditional methods to identify writers and erasers, including overexpression and knockdown of said proteins, failed to reveal DHHC and APT regulators of ERK *S*-acylation. This result emphasizes that identification of molecular determinants for a substrate whose steady-state *S*-acylation status is tightly regulated by multiple actors requires different experimental approaches. In the case of ERK2, chemical metabolic labeling enabled observation of changes in palmitate incorporation with DHHC overexpression, while co-immunoprecipitation validated DHHC/ERK2 interactions and the phosphorylation change assay the role of DHHCs in ERK2 activation. The observation of dynamic interactions between ERK2 and DHHCs/APT2 in the context of EGF stimulation is also noteworthy. While steady-state substrate-writer/eraser associations are well established (e.g., STAT3/DHHC7 and Scribble/APT2), here we find that interactions between ERK2 and DHHCs/APT2 are sensitive to EGF signaling.[7,74] This again hints at upstream crosstalk between dynamic phosphorylation and *S*-acylation, and although the mechanisms that drive these interactions have yet to be elucidated, it also spotlights the importance of exploring dynamic interactions in changing cellular contexts for other *S*-acylated substrates.

In identifying ERK1/2 *S*-acylation writers, we also observed that certain DHHC-family proteins, including 9, 23, 12, 15, and 20, appeared to affect *S*-acylation of ERK1 more significantly than that of ERK2 (Figure 5A). These results suggest a possible ERK isoform-specific mode of regulation and highlight the potential of isoform-selective DHHC inhibitors to modulate ERK1 vs. ERK2 signaling. In addition, the efficacy of CMA as a chemical inhibitor of ERK1/2 *S*-acylation, in contrast to the well-established 2BP, emphasizes the potential utility of new broad-spectrum DHHC-family inhibitors. Also interesting was ERK2's association with zDHHC5 (Figure S5E). This plasma-membrane-localized PAT is unlikely to be a writer of ERK1/2 *S*-acylation, given its inability to increase fatty acid incorporation (Figure 5A).[52] However, proximity proteomics experiments indicate that it is associated with Grb2, an adaptor protein that links the MAPK pathway to activated RTKs.[75] These associations suggest that it may have a role as a scaffolding protein in the EGFR signaling complex.

The observation of organ-specific changes in ERK1/2 *S*-acylation in a mouse model of metabolic syndrome underscores the responsiveness of this modification to the organismal environment and its potential as a regulatory mechanism (Figure 6). Given our data suggesting that ERK1/2 acylation status regulates their activity and stability, this result strongly suggests that *S*-acylation could be a significant contributor to altered ERK1/2 signaling in metabolic syndrome. The alterations in expression of *S*-acylation writers and erasers suggest that the acylation machinery is sensitive to metabolic stress, an observation with implications not only for ERK1/2 but also for the thousands of proteins whose activity is regulated by enzymatic *S*-acylation.

Overall, this works helps to address the still salient question for ERK1/2—*quis regit ipsos regendos*/who regulates the regulators?—by adding a new element to regulation of ERK1/2 and presenting a new therapeutic hypothesis for targeting ERK1/2-driven pathologies. More broadly, this work highlights the connection between dynamic lipidation and phosphorylation, a connection hinted at by our previous work showing that APT activity is responsive to growth factor stimulation and lipid stress and by the observation that APT1 activity is regulated by phosphorylation.[70,72,73] It also underscores the importance of timing and cell state in identifying the molecular determinants and significance of *S*-acylation for a substrate, especially given the observation of dynamic interactions between ERK2 and APT2/DHHCs. Further exploration of the mechanisms that regulate the dynamic activity and interactions of acylation writer/eraser proteins will broaden our perspective on the regulatory machinery of the cell in physiological and pathological contexts. Overall, this work and the approaches described here grow our understanding of dynamic protein *S*-acylation and provide a roadmap to further deconvolute the role of dynamic *S*-acylation in regulating signal transduction.

Limitations of the study

While it is clear that *S*-acylation is significant for ERK1/2 activity, there are limitations to the present study. First, many observations relating ERK2 acylation to its activity and interaction partners were made using the acylation-deficient mutant. Ideally, these observations would be validated via manipulation of writer enzymes, but the number of identified writers precluded significant changes in lipidation status with single-protein siRNA knockdown. While some results were validated using chemical inhibitors, these small molecules are non-selective, complicating interrogation of downstream consequences. More broadly, the precise mechanism orchestrating phosphorylation and ERK activity changes in response to *S*-acylation changes remains somewhat obscure; of particular interest will be further work evaluating ERK1/2 nuclear translocation/transcriptional changes and their connection with lipidation. Finally, the correlations between ERK2 *S*-acylation and activity in a mouse model of metabolic disease are evocative, but missing are data showing that *S*-acylation is the molecular link between changes in diet and changes in ERK1/2 activity.

STAR★METHODS

Detailed methods are provided in the online version of this paper and include the following:

- KEY RESOURCES TABLE
- RESOURCE AVAILABILITY
  - Lead contact
  - Materials availability
  - Data and code availability
- EXPERIMENTAL MODEL AND STUDY PARTICIPANT DETAILS
  - Cell culture
  - Mouse models
- METHOD DETAILS
  - Plasmid cloning
  - Western blotting
  - Acyl biotin exchange (ABE)
  - Metabolic labeling

- Immunoprecipitations
- RT-qPCR
- TurboID

- QUANTIFICATION AND STATISTICAL ANALYSIS

SUPPLEMENTAL INFORMATION

Supplemental information can be found online at https://doi.org/10.1016/j.celrep.2023.113135.

ACKNOWLEDGMENTS

This research was supported by the University of Chicago, the National Institute of General Medical Sciences of the National Institutes of Health (NIH; R35 GM119840 to B.C.D.), and the National Institute of Diabetes and Digestive and Kidney Diseases of the National Institutes of Health (F30 DK125088 to S.-A.A.). We thank the Fukata lab for providing the HA-tagged mDHHC plasmids. We would also like to thank Dr. S. Ahmadiantehrani and Prof. Marsha Rosner for assistance with preparing this manuscript, and Dr. M. Beck for early input for this project.

AUTHOR CONTRIBUTIONS

S-A.A. designed and conducted experiments, analyzed data, assembled figures, and wrote the original manuscript. T.Q. performed experiments, analyzed data, and assisted with assembly of figures and writing of the text. N.B. conducted experiments and analyzed data. B.C.D. designed and supervised experiments and assisted with assembly of the manuscript text and figures.

DECLARATION OF INTERESTS

The authors declare no competing interests.

INCLUSION AND DIVERSITY

We support inclusive, diverse, and equitable conduct of research.

Received: April 6, 2023
Revised: July 28, 2023
Accepted: August 30, 2023

REFERENCES

1. Jiang, H., Zhang, X., Chen, X., Aramsangtienchai, P., Tong, Z., and Lin, H. (2018). Protein Lipidation: Occurrence, Mechanisms, Biological Functions, and Enabling Technologies. Chem. Rev. *118*, 919–988. https://doi.org/10.1021/acs.chemrev.6b00750.
2. Chamberlain, L.H., and Shipston, M.J. (2015). The physiology of protein S-acylation. Physiol. Rev. *95*, 341–376. https://doi.org/10.1152/physrev.00032.2014.
3. Chen, S., Zhu, B., Yin, C., Liu, W., Han, C., Chen, B., Liu, T., Li, X., Chen, X., Li, C., et al. (2017). Palmitoylation-dependent activation of MC1R prevents melanomagenesis. Nature *549*, 399–403. https://doi.org/10.1038/nature23887.
4. Runkle, K.B., Kharbanda, A., Stypulkowski, E., Cao, X.J., Wang, W., Garcia, B.A., and Witze, E.S. (2016). Inhibition of DHHC20-Mediated EGFR Palmitoylation Creates a Dependence on EGFR Signaling. Mol. Cell *62*, 385–396. https://doi.org/10.1016/j.molcel.2016.04.003.
5. Blaustein, M., Piegari, E., Martínez Calejman, C., Vila, A., Amante, A., Manese, M.V., Zeida, A., Abrami, L., Veggetti, M., Guertin, D.A., et al. (2021). Akt Is S-Palmitoylated: A New Layer of Regulation for Akt. Front. Cell Dev. Biol. *9*, 626404. https://doi.org/10.3389/fcell.2021.626404.
6. Yang, G., Liu, Y., Yang, K., Liu, R., Zhu, S., Coquinco, A., Wen, W., Kojic, L., Jia, W., and Cynader, M. (2012). Isoform-specific palmitoylation of JNK regulates axonal development. Cell Death Differ. *19*, 553–561. https://doi.org/10.1038/cdd.2011.124.
7. Zhang, M., Zhou, L., Xu, Y., Yang, M., Xu, Y., Komaniecki, G.P., Kosciuk, T., Chen, X., Lu, X., Zou, X., et al. (2020). A STAT3 palmitoylation cycle promotes TH17 differentiation and colitis. Nature *586*, 434–439. https://doi.org/10.1038/s41586-020-2799-2.
8. Cargnello, M., and Roux, P.P. (2011). Activation and function of the MAPKs and their substrates, the MAPK-activated protein kinases. Microbiol. Mol. Biol. Rev. *75*, 50–83. https://doi.org/10.1128/MMBR.00031-10.
9. Morrison, D.K. (2012). MAP kinase pathways. Cold Spring Harb. Perspect. Biol. *4*, a011254. https://doi.org/10.1101/cshperspect.a011254.
10. Lavoie, H., Gagnon, J., and Therrien, M. (2020). ERK signalling: a master regulator of cell behaviour, life and fate. Nat. Rev. Mol. Cell Biol. *21*, 607–632. https://doi.org/10.1038/s41580-020-0255-7.
11. Chang, F., Steelman, L.S., Lee, J.T., Shelton, J.G., Navolanic, P.M., Blalock, W.L., Franklin, R.A., and McCubrey, J.A. (2003). Signal transduction mediated by the Ras/Raf/MEK/ERK pathway from cytokine receptors to transcription factors: potential targeting for therapeutic intervention. Leukemia *17*, 1263–1293. https://doi.org/10.1038/sj.leu.2402945.
12. Sun, Y., Liu, W.Z., Liu, T., Feng, X., Yang, N., and Zhou, H.F. (2015). Signaling pathway of MAPK/ERK in cell proliferation, differentiation, migration, senescence and apoptosis. J. Recept. Signal Transduct. Res. *35*, 600–604. https://doi.org/10.3109/10799893.2015.1030412.
13. Papa, S., Choy, P.M., and Bubici, C. (2019). The ERK and JNK pathways in the regulation of metabolic reprogramming. Oncogene *38*, 2223–2240. https://doi.org/10.1038/s41388-018-0582-8.
14. Ebisuya, M., Kondoh, K., and Nishida, E. (2005). The duration, magnitude and compartmentalization of ERK MAP kinase activity: mechanisms for providing signaling specificity. J. Cell Sci. *118*, 2997–3002. https://doi.org/10.1242/jcs.02505.
15. Wortzel, I., and Seger, R. (2011). The ERK Cascade: Distinct Functions within Various Subcellular Organelles. Genes Cancer *2*, 195–209. https://doi.org/10.1177/1947601911407328.
16. Lake, D., Corrêa, S.A.L., and Müller, J. (2016). Negative feedback regulation of the ERK1/2 MAPK pathway. Cell. Mol. Life Sci. *73*, 4397–4413. https://doi.org/10.1007/s00018-016-2297-8.
17. Chuderland, D., Konson, A., and Seger, R. (2008). Identification and characterization of a general nuclear translocation signal in signaling proteins. Mol. Cell *31*, 850–861. https://doi.org/10.1016/j.molcel.2008.08.007.
18. Oppermann, F.S., Gnad, F., Olsen, J.V., Hornberger, R., Greff, Z., Kéri, G., Mann, M., and Daub, H. (2009). Large-scale proteomics analysis of the human kinome. Mol. Cell. Proteomics *8*, 1751–1764. https://doi.org/10.1074/mcp.M800588-MCP200.
19. Berti, D.A., and Seger, R. (2017). The Nuclear Translocation of ERK. Methods Mol. Biol. *1487*, 175–194. https://doi.org/10.1007/978-1-4939-6424-6_13.
20. Feng, X., Sun, T., Bei, Y., Ding, S., Zheng, W., Lu, Y., and Shen, P. (2013). S-nitrosylation of ERK inhibits ERK phosphorylation and induces apoptosis. Sci. Rep. *3*, 1814. https://doi.org/10.1038/srep01814.
21. Wu, J.Y., Xiang, S., Zhang, M., Fang, B., Huang, H., Kwon, O.K., Zhao, Y., Yang, Z., Bai, W., Bepler, G., and Zhang, X.M. (2018). Histone deacetylase 6 (HDAC6) deacetylates extracellular signal-regulated kinase 1 (ERK1) and thereby stimulates ERK1 activity. J. Biol. Chem. *293*, 1976–1993. https://doi.org/10.1074/jbc.M117.795955.
22. Vougiouklakis, T., Sone, K., Saloura, V., Cho, H.S., Suzuki, T., Dohmae, N., Alachkar, H., Nakamura, Y., and Hamamoto, R. (2015). SUV420H1 enhances the phosphorylation and transcription of ERK1 in cancer cells. Oncotarget *6*, 43162–43171. https://doi.org/10.18632/oncotarget.6351.
23. Shaul, Y.D., and Seger, R. (2007). The MEK/ERK cascade: from signaling specificity to diverse functions. Biochim. Biophys. Acta *1773*, 1213–1226. https://doi.org/10.1016/j.bbamcr.2006.10.005.

24. Raman, M., Chen, W., and Cobb, M.H. (2007). Differential regulation and properties of MAPKs. Oncogene *26*, 3100–3112. https://doi.org/10.1038/sj.onc.1210392.

25. Katz, M., Amit, I., and Yarden, Y. (2007). Regulation of MAPKs by growth factors and receptor tyrosine kinases. Biochim. Biophys. Acta *1773*, 1161–1176. https://doi.org/10.1016/j.bbamcr.2007.01.002.

26. Buscà, R., Pouysségur, J., and Lenormand, P. (2016). ERK1 and ERK2 Map Kinases: Specific Roles or Functional Redundancy? Front. Cell Dev. Biol. *4*, 53. https://doi.org/10.3389/fcell.2016.00053.

27. Ren, W., Jhala, U.S., and Du, K. (2013). Proteomic analysis of protein palmitoylation in adipocytes. Adipocyte *2*, 17–28. https://doi.org/10.4161/adip.22117.

28. Drisdel, R.C., and Green, W.N. (2004). Labeling and quantifying sites of protein palmitoylation. Biotechniques *36*, 276–285. https://doi.org/10.2144/04362RR02.

29. Charron, G., Zhang, M.M., Yount, J.S., Wilson, J., Raghavan, A.S., Shamir, E., and Hang, H.C. (2009). Robust fluorescent detection of protein fatty-acylation with chemical reporters. J. Am. Chem. Soc. *131*, 4967–4975. https://doi.org/10.1021/ja810122f.

30. Kiyatkin, A., van Alderwerelt van Rosenburgh, I.K., Klein, D.E., and Lemmon, M.A. (2020). Kinetics of receptor tyrosine kinase activation define ERK signaling dynamics. Sci. Signal. *13*, eaaz5267. https://doi.org/10.1126/scisignal.aaz5267.

31. Pinilla-Macua, I., Grassart, A., Duvvuri, U., Watkins, S.C., and Sorkin, A. (2017). EGF receptor signaling, phosphorylation, ubiquitylation and endocytosis in tumors in vivo. Elife *6*, e31993. https://doi.org/10.7554/eLife.31993.

32. Tai, W.M., Yong, W.P., Lim, C., Low, L.S., Tham, C.K., Koh, T.S., Ng, Q.S., Wang, W.W., Wang, L.Z., Hartano, S., et al. (2016). A phase Ib study of selumetinib (AZD6244, ARRY-142886) in combination with sorafenib in advanced hepatocellular carcinoma (HCC). Ann. Oncol. *27*, 2210–2215. https://doi.org/10.1093/annonc/mdw415.

33. Sebolt-Leopold, J.S., Dudley, D.T., Herrera, R., Van Becelaere, K., Wiland, A., Gowan, R.C., Tecle, H., Barrett, S.D., Bridges, A., Przybranowski, S., et al. (1999). Blockade of the MAP kinase pathway suppresses growth of colon tumors in vivo. Nat. Med. *5*, 810–816. https://doi.org/10.1038/10533.

34. Tsai, J., Lee, J.T., Wang, W., Zhang, J., Cho, H., Mamo, S., Bremer, R., Gillette, S., Kong, J., Haass, N.K., et al. (2008). Discovery of a selective inhibitor of oncogenic B-Raf kinase with potent antimelanoma activity. Proc. Natl. Acad. Sci. USA *105*, 3041–3046. https://doi.org/10.1073/pnas.0711741105.

35. Cohen, P., Klumpp, S., and Schelling, D.L. (1989). An improved procedure for identifying and quantitating protein phosphatases in mammalian tissues. FEBS Lett. *250*, 596–600. https://doi.org/10.1016/0014-5793(89)80803-8.

36. Peti, W., and Page, R. (2013). Molecular basis of MAP kinase regulation. Protein Sci. *22*, 1698–1710. https://doi.org/10.1002/pro.2374.

37. Kutzleb, C., Sanders, G., Yamamoto, R., Wang, X., Lichte, B., Petrasch-Parwez, E., and Kilimann, M.W. (1998). Paralemmin, a prenyl-palmitoyl-anchored phosphoprotein abundant in neurons and implicated in plasma membrane dynamics and cell process formation. J. Cell Biol. *143*, 795–813. https://doi.org/10.1083/jcb.143.3.795.

38. Borgo, C., D'Amore, C., Sarno, S., Salvi, M., and Ruzzene, M. (2021). Protein kinase CK2: a potential therapeutic target for diverse human diseases. Signal Transduct. Target. Ther. *6*, 183. https://doi.org/10.1038/s41392-021-00567-7.

39. Plotnikov, A., Chuderland, D., Karamansha, Y., Livnah, O., and Seger, R. (2019). Nuclear ERK Translocation is Mediated by Protein Kinase CK2 and Accelerated by Autophosphorylation. Cell. Physiol. Biochem. *53*, 366–387. https://doi.org/10.33594/000000144.

40. Cho, K.F., Branon, T.C., Udeshi, N.D., Myers, S.A., Carr, S.A., and Ting, A.Y. (2020). Proximity labeling in mammalian cells with TurboID and split-TurboID. Nat. Protoc. *15*, 3971–3999. https://doi.org/10.1038/s41596-020-0399-0.

41. Plotnikov, A., Flores, K., Maik-Rachline, G., Zehorai, E., Kapri-Pardes, E., Berti, D.A., Hanoch, T., Besser, M.J., and Seger, R. (2015). The nuclear translocation of ERK1/2 as an anticancer target. Nat. Commun. *6*, 6685. https://doi.org/10.1038/ncomms7685.

42. Niphakis, M.J., Lum, K.M., Cognetta, A.B., 3rd, Correia, B.E., Ichu, T.A., Olucha, J., Brown, S.J., Kundu, S., Piscitelli, F., Rosen, H., and Cravatt, B.F. (2015). A Global Map of Lipid-Binding Proteins and Their Ligandability in Cells. Cell *161*, 1668–1680. https://doi.org/10.1016/j.cell.2015.05.045.

43. Bolognesi, B., and Lehner, B. (2018). Reaching the limit. Elife *7*, e39804. https://doi.org/10.7554/eLife.39804.

44. Webb, Y., Hermida-Matsumoto, L., and Resh, M.D. (2000). Inhibition of protein palmitoylation, raft localization, and T cell signaling by 2-bromopalmitate and polyunsaturated fatty acids. J. Biol. Chem. *275*, 261–270. https://doi.org/10.1074/jbc.275.1.261.

45. Azizi, S.-A., Lan, T., Delalande, C., Kathayat, R.S., Banales Mejia, F., Qin, A., Brookes, N., Sandoval, P.J., and Dickinson, B.C. (2021). Development of an Acrylamide-Based Inhibitor of Protein S-Acylation. ACS Chem. Biol. *16*, 1546–1556. https://doi.org/10.1021/acschembio.1c00405.

46. Lan, T., Delalande, C., and Dickinson, B.C. (2021). Inhibitors of DHHC family proteins. Curr. Opin. Chem. Biol. *65*, 118–125. https://doi.org/10.1016/j.cbpa.2021.07.002.

47. Dekker, F.J., Rocks, O., Vartak, N., Menninger, S., Hedberg, C., Balamurugan, R., Wetzel, S., Renner, S., Gerauer, M., Schölermann, B., et al. (2010). Small-molecule inhibition of APT1 affects Ras localization and signaling. Nat. Chem. Biol. *6*, 449–456. https://doi.org/10.1038/nchembio.362.

48. Adibekian, A., Martin, B.R., Chang, J.W., Hsu, K.L., Tsuboi, K., Bachovchin, D.A., Speers, A.E., Brown, S.J., Spicer, T., Fernandez-Vega, V., et al. (2010). Characterization of a Selective, Reversible Inhibitor of Lysophospholipase 1 (LYPLA1). In Probe Reports from the NIH Molecular Libraries Program.

49. Adibekian, A., Martin, B.R., Chang, J.W., Hsu, K.L., Tsuboi, K., Bachovchin, D.A., Speers, A.E., Brown, S.J., Spicer, T., Fernandez-Vega, V., et al. (2010). Characterization of a Selective, Reversible Inhibitor of Lysophospholipase 2 (LYPLA2). In Probe Reports from the NIH Molecular Libraries Program.

50. Uhlitz, F., Sieber, A., Wyler, E., Fritsche-Guenther, R., Meisig, J., Landthaler, M., Klinger, B., and Blüthgen, N. (2017). An immediate-late gene expression module decodes ERK signal duration. Mol. Syst. Biol. *13*, 928. https://doi.org/10.15252/msb.20177554.

51. Fukata, Y., Iwanaga, T., and Fukata, M. (2006). Systematic screening for palmitoyl transferase activity of the DHHC protein family in mammalian cells. Methods *40*, 177–182. https://doi.org/10.1016/j.ymeth.2006.05.015.

52. Ohno, Y., Kihara, A., Sano, T., and Igarashi, Y. (2006). Intracellular localization and tissue-specific distribution of human and yeast DHHC cysteine-rich domain-containing proteins. Biochim. Biophys. Acta *1761*, 474–483. https://doi.org/10.1016/j.bbalip.2006.03.010.

53. Lin, D.T.S., and Conibear, E. (2015). ABHD17 proteins are novel protein depalmitoylases that regulate N-Ras palmitate turnover and subcellular localization. Elife *4*, e11306. https://doi.org/10.7554/eLife.11306.

54. Cao, Y., Qiu, T., Kathayat, R.S., Azizi, S.A., Thorne, A.K., Ahn, D., Fukata, Y., Fukata, M., Rice, P.A., and Dickinson, B.C. (2019). ABHD10 is an S-depalmitoylase affecting redox homeostasis through peroxiredoxin-5. Nat. Chem. Biol. *15*, 1232–1240. https://doi.org/10.1038/s41589-019-0399-y.

55. Azizi, S.A., Kathayat, R.S., and Dickinson, B.C. (2019). Activity-Based Sensing of S-Depalmitoylases: Chemical Technologies and Biological Discovery. Acc. Chem. Res. *52*, 3029–3038. https://doi.org/10.1021/acs.accounts.9b00354.

56. Gehart, H., Kumpf, S., Ittner, A., and Ricci, R. (2010). MAPK signalling in cellular metabolism: stress or wellness? EMBO Rep. *11*, 834–840. https://doi.org/10.1038/embor.2010.160.

57. Ozaki, K.I., Awazu, M., Tamiya, M., Iwasaki, Y., Harada, A., Kugisaki, S., Tanimura, S., and Kohno, M. (2016). Targeting the ERK signaling pathway as a potential treatment for insulin resistance and type 2 diabetes. Am. J. Physiol. Endocrinol. Metab. *310*, E643–E651. https://doi.org/10.1152/ajpendo.00445.2015.

58. Spinelli, M., Fusco, S., and Grassi, C. (2018). Nutrient-Dependent Changes of Protein Palmitoylation: Impact on Nuclear Enzymes and Regulation of Gene Expression. Int. J. Mol. Sci. *19*, 3820. https://doi.org/10.3390/ijms19123820.

59. Wang, C.Y., and Liao, J.K. (2012). A mouse model of diet-induced obesity and insulin resistance. Methods Mol. Biol. *821*, 421–433. https://doi.org/10.1007/978-1-61779-430-8_27.

60. Bi, L., Chiang, J.Y.L., Ding, W.X., Dunn, W., Roberts, B., and Li, T. (2013). Saturated fatty acids activate ERK signaling to downregulate hepatic sortilin 1 in obese and diabetic mice. J. Lipid Res. *54*, 2754–2762. https://doi.org/10.1194/jlr.M039347.

61. Bost, F., Aouadi, M., Caron, L., Even, P., Belmonte, N., Prot, M., Dani, C., Hofman, P., Pagès, G., Pouysségur, J., et al. (2005). The extracellular signal-regulated kinase isoform ERK1 is specifically required for in vitro and in vivo adipogenesis. Diabetes *54*, 402–411. https://doi.org/10.2337/diabetes.54.2.402.

62. Karmi, A., Iozzo, P., Viljanen, A., Hirvonen, J., Fielding, B.A., Virtanen, K., Oikonen, V., Kemppainen, J., Viljanen, T., Guiducci, L., et al. (2010). Increased brain fatty acid uptake in metabolic syndrome. Diabetes *59*, 2171–2177. https://doi.org/10.2337/db09-0138.

63. Guo, S. (2014). Insulin signaling, resistance, and the metabolic syndrome: insights from mouse models into disease mechanisms. J. Endocrinol. *220*, T1–T23. https://doi.org/10.1530/JOE-13-0327.

64. Jiao, P., Feng, B., Li, Y., He, Q., and Xu, H. (2013). Hepatic ERK activity plays a role in energy metabolism. Mol. Cell. Endocrinol. *375*, 157–166. https://doi.org/10.1016/j.mce.2013.05.021.

65. Brown, J.M., Bentsen, M.A., Rausch, D.M., Phan, B.A., Wieck, D., Wasanwala, H., Matsen, M.E., Acharya, N., Richardson, N.E., Zhao, X., et al. (2021). Role of hypothalamic MAPK/ERK signaling and central action of FGF1 in diabetes remission. iScience *24*, 102944. https://doi.org/10.1016/j.isci.2021.102944.

66. Roskoski, R., Jr. (2012). ERK1/2 MAP kinases: structure, function, and regulation. Pharmacol. Res. *66*, 105–143. https://doi.org/10.1016/j.phrs.2012.04.005.

67. Miao, L., and Tian, H. (2020). Development of ERK1/2 inhibitors as a therapeutic strategy for tumour with MAPK upstream target mutations. J. Drug Target. *28*, 154–165. https://doi.org/10.1080/1061186X.2019.1648477.

68. Sun, J., and Nan, G. (2017). The extracellular signal-regulated kinase 1/2 pathway in neurological diseases: A potential therapeutic target (Review). Int. J. Mol. Med. *39*, 1338–1346. https://doi.org/10.3892/ijmm.2017.2962.

69. Lu, N., and Malemud, C.J. (2019). Extracellular Signal-Regulated Kinase: A Regulator of Cell Growth, Inflammation, Chondrocyte and Bone Cell Receptor-Mediated Gene Expression. Int. J. Mol. Sci. *20*, 3792. https://doi.org/10.3390/ijms20153792.

70. Kathayat, R.S., Elvira, P.D., and Dickinson, B.C. (2017). A fluorescent probe for cysteine depalmitoylation reveals dynamic APT signaling. Nat. Chem. Biol. *13*, 150–152. https://doi.org/10.1038/nchembio.2262.

71. Beck, M.W., Kathayat, R.S., Cham, C.M., Chang, E.B., and Dickinson, B.C. (2017). Michael addition-based probes for ratiometric fluorescence imaging of protein S-depalmitoylases in live cells and tissues. Chem. Sci. *8*, 7588–7592. https://doi.org/10.1039/c7sc02805a.

72. Qiu, T., Kathayat, R.S., Cao, Y., Beck, M.W., and Dickinson, B.C. (2018). A Fluorescent Probe with Improved Water Solubility Permits the Analysis of Protein S-Depalmitoylation Activity in Live Cells. Biochemistry *57*, 221–225. https://doi.org/10.1021/acs.biochem.7b00835.

73. Sadeghi, R.S., Kulej, K., Kathayat, R.S., Garcia, B.A., Dickinson, B.C., Brady, D.C., and Witze, E.S. (2018). Wnt5a signaling induced phosphorylation increases APT1 activity and promotes melanoma metastatic behavior. Elife *7*, e34362. https://doi.org/10.7554/eLife.34362.

74. Hernandez, J.L., Davda, D., Cheung See Kit, M., Majmudar, J.D., Won, S.J., Gang, M., Pasupuleti, S.C., Choi, A.I., Bartkowiak, C.M., and Martin, B.R. (2017). APT2 Inhibition Restores Scribble Localization and S-Palmitoylation in Snail-Transformed Cells. Cell Chem. Biol. *24*, 87–97. https://doi.org/10.1016/j.chembiol.2016.12.007.

75. Ke, M., Yuan, X., He, A., Yu, P., Chen, W., Shi, Y., Hunter, T., Zou, P., and Tian, R. (2021). Spatiotemporal profiling of cytosolic signaling complexes in living cells by selective proximity proteomics. Nat. Commun. *12*, 71. https://doi.org/10.1038/s41467-020-20367-x.

76. Schneider, C.A., Rasband, W.S., and Eliceiri, K.W. (2012). NIH Image to ImageJ: 25 years of image analysis. Nat. Methods *9*, 671–675. https://doi.org/10.1038/nmeth.2089.

STAR★METHODS

KEY RESOURCES TABLE

REAGENT or RESOURCE	SOURCE	IDENTIFIER
Antibodies		
Rabbit anti-ERK1/2 (p44/42 MAPK)	Cell Signaling Technology	9102S; RRID: AB_330744
Rabbit anti-Phospho-ERK1/2 (Thr202/Tyr204)	Cell Signaling Technology	9101S; RRID: AB_331772
Mouse anti-*c*-Myc (9E10)	Santa Cruz Biotechnology	sc-40; RRID: AB_2857941
Mouse anti-FLAG (DYKDDDDK; FG4R)	Invitrogen	MA1-91878; RRID: AB_2537622
Rabbit anti-APT1 (LPL-I; EPR3667)	Abcam	AB-91606; RRID: AB_10565192
Rabbit anti-APT2	Abcam	AB-151578; Not available
Mouse anti-HA-Tag (F-7)	Santa Cruz Biotechnology	sc-7392; RRID: AB_627809
Rabbit anti-Phosphoserine	Abcam	AB-9332; RRID: AB_307184
Rabbit anti-Calnexin	Abcam	AB-22595; RRID: AB_2069006
Chemicals, peptides, and recombinant proteins		
2-bromopalmitate	Sigma-Aldrich	21604; CAS: 18263-25-7
Palmostatin B	Sigma-Aldrich	178501
ML-348	Tocris	5345; CAS: 899713-86-1
ML-349	Tocris	5344; CAS: 890819-86-0
N-ethylmaleimide	Acros	156100050; CAS: 128-53-0
EZ-Link™ HPDP-Biotin	ThermoFisher	Cat# 21341
Streptavidin-Peroxidase Polymer	Sigma-Aldrich	Cat# S2438
Phosphatase Inhibitor Cocktail A	Santa Cruz Biotechnology	Cat# sc-45044
Phosphatase Inhibitor Cocktail B	Santa Cruz Biotechnology	Cat# sc-45045
Protein G Dynabeads	Invitrogen	Cat# 10003D
Critical commercial assays		
BCA Protein Assay Kit	ThermoFisher	Cat# J63283.QA
RNeasy Mini Kit	Qiagen	Cat# 74106
RNA Clean & Concentrator kit	Zymo Research	Cat# R1014
PrimeScript RT Reagent Kit	TaKaRa Bio	Cat# RR037B
PowerUp SYBR Green Master Mix	Applied Biosystems	Cat# A25777
Experimental models: Cell lines		
Human: HEK293T cells	ATCC	CRL-3216; RRID:CVCL_0063
Human: A-431cells	ATCC	CRL-1555; RRID:CVCL_0037
Human: Hep G2 cells	ATCC	HB-8065; RRID:CVCL_0027
Experimental models: Organisms/strains		
Mouse: DIO	Jackson Labs	Stock No.: 380050 RRID:IMSR_JAX:380050
Mouse: DIO control	Jackson Labs	Stock No.: 380056 RRID:IMSR_JAX:380056
Oligonucleotides		
Hs_LYPLA1_6 FlexiTube siRNA (human APT1/LYPLA1 siRNA)	Qiagen	GeneGlobe ID: SI03246586
Hs_LYPLA2_9 FlexiTube siRNA (human APT2/LYPLA2 siRNA)	Qiagen	GeneGlobe ID: SI04269041
Negative Control (nontargeting; NT) siRNA	Qiagen	GeneGlobe ID: SI03650325
F Primer: cFos 5′-CAAGCGGAGACAGACCAACT-3′	Integrated DNA Technologies	N/A
R Primer: cFos 5′-AGTCAGATCAAGGGAAGCCA-3′	Integrated DNA Technologies	N/A
F Primer: EGR1 5′-CAGCACCTTCAACCCTCAG-3′	Integrated DNA Technologies	N/A

(*Continued on next page*)

Continued

REAGENT or RESOURCE	SOURCE	IDENTIFIER
R Primer: EGR1 5′-AGCGGCCAGTATAGGTGATG-3′	Integrated DNA Technologies	N/A
F Primer: EGR2 5′-CCTTTGACCAGATGAACGGAGTG-3′	Integrated DNA Technologies	N/A
R Primer: EGR2 5′-GAAGGTCTGGTTTCTAGGTGCAG-3′	Integrated DNA Technologies	N/A
F Primer: DUSP1 5′-CAACCACAAGGCAGACATCAGC-3′	Integrated DNA Technologies	N/A
R Primer: DUSP1 5′-GTAAGCAAGGCAGATGGTGGCT-3′	Integrated DNA Technologies	N/A
F Primer: DUSP6 5′-TCCCTGAGGCCATTTCTTTCATAGATG-3′	Integrated DNA Technologies	N/A
R Primer: DUSP6 5′-GCAGCTGACCCATGAAGTTGAAGT-3′	Integrated DNA Technologies	N/A
F Primer: mDHHC3 5′-TGGTGGGATTCCACTTCCTGCA-3′	Integrated DNA Technologies	N/A
R Primer: mDHHC3 5′-GCCTCAAAGCACAGCAGGATGA-3′	Integrated DNA Technologies	N/A
F Primer: mDHHC7 5′-GCTCTGTCTTCGGTTCATGCTC-3′	Integrated DNA Technologies	N/A
R Primer: mDHHC7 5′-CTCAAGGCACAGGAAGACCAAC-3′	Integrated DNA Technologies	N/A
F Primer: mDHHC9 5′-CTGCTGTGAAGTGCTTTGTGGC-3′	Integrated DNA Technologies	N/A
R Primer: mDHHC9 5′-TCTGTGGCAACAGGCTACTGCT-3′	Integrated DNA Technologies	N/A
F Primer: mDHHC14 5′-ACAGAAGAGGCTATGTCCAGCC-3′	Integrated DNA Technologies	N/A
R Primer: mDHHC14 5′-GCTCTGAATGCACTGGTCTTGG-3′	Integrated DNA Technologies	N/A
F Primer: mDHHC17 5′-CTTCCTTGCCAACAGCGTTGCT-3′	Integrated DNA Technologies	N/A
R Primer: mDHHC17 5′-TGAGGTCCAGACTTCCAGTCTC-3′	Integrated DNA Technologies	N/A
F Primer: mDHHC21 5′-CTGAGCTGCTTACTTGCTACGC-3′	Integrated DNA Technologies	N/A
R Primer: mDHHC21 5′-TGCCCATGAAGGCAGCTAGTCT-3′	Integrated DNA Technologies	N/A
F Primer: mDHHC23 5′-GGATATGCGGTATCTGTGTACGG-3′	Integrated DNA Technologies	N/A
F Primer: mDHHC23 5′-GGTCAGCGATATTCCGTAAACCG-3′	Integrated DNA Technologies	N/A
F Primer: mLYPLA1 5′-CTCACCACACAGCAGAAACTGG-3′	Integrated DNA Technologies	N/A
R Primer: mLYPLA1 5′-TCCATGGCACTGGAGAACGGAA-3′	Integrated DNA Technologies	N/A
F Primer: mLYPLA2 5′-CCTCTATACAGCACTTACCTGCC-3′	Integrated DNA Technologies	N/A
R Primer: mLYPLA2 5′-CAGGTCCTTGGCACTGCCATTG-3′	Integrated DNA Technologies	N/A
Recombinant DNA		
pFLAG-CMV-hErk1	Addgene	RRID:Addgene_49328

(*Continued on next page*)

Continued

REAGENT or RESOURCE	SOURCE	IDENTIFIER
pDONR223_MAPK1_WT	Addgene	RRID:Addgene_82145
Flag-TurboID	Addgene	RRID:Addgene_124646
mDHHC plasmids	Masaki Fukata	Fukata et al., 2006
Software and algorithms		
Leica LASX software	Leica	Leica Application Suite X (RRID:SCR_013673)
ImageJ	Schneider et al., 2012[76]	https://imagej.nih.gov/ij/
GraphPad Prism9	GraphPad Software	RRID: SCR_002798
Other		
PEI Prime™ linear polyethylenimine	Sigma-Aldrich	Cat# 919012
Lipofectamine™ 3000 Transfection Reagent	Invitrogen	Cat# L3000
High fat diet	Research Diets, Inc.	D12492
Control diet	Research Diets, Inc.	D12450B

RESOURCE AVAILABILITY

Lead contact

Further information and requests for resources and reagents should be directed to and will be fulfilled by the lead contact, Bryan C. Dickinson (dickinson@uchicago.edu).

Materials availability

This study did not generate new unique reagents.

Data and code availability

- All data reported in this paper will be shared by the lead contact upon request.
- This paper does not report original code.
- Any additional information required to reanalyze the data reported in this work paper is available from the lead contact upon request.

EXPERIMENTAL MODEL AND STUDY PARTICIPANT DETAILS

Cell culture

Cells were plated and maintained in growth media (DMEM GlutaMAX for HEK293T and A431cells; EMEM for HepG2 cells) supplemented with 10% FBS and 1% penicillin/streptomycin at 37°C and 5% CO_2. For all experiments, cells had undergone fewer than 18 passages. Transfections were conducted using PEI (Sigma) or Lipofectamine 3000 (Invitrogen) in accordance with manufacturer protocols.

Mouse models

The use of vertebrate animals (*Mus musculus*, mouse) in the laboratory of B. Dickinson has been approved by the Institutional Animal Care and Use Committee under the Animal Care and Use protocol no. 72531, 'Mouse models of lipid signaling regulation'. DIO or DIO control mice (male, 5× each) were purchased from Jackson Labs (see key resources table) at 12 weeks of age and then maintained on either the high fat diet (60 kcal% fat) or the control diet (10 kcal% fat) (Research Diets, Inc.; see key resources table) for an additional 6 weeks. To confirm the manifestation of metabolic syndrome, insulin tolerance tests (ITT) and glucose tolerance tests (GTT) were carried out in accordance with previously reported protocols (Wang and Liao, 2012).

METHOD DETAILS

Plasmid cloning

All plasmids were constructed by Gibson Assembly from PCR products generated using Q5 Hot Start DNA Polymerase (New England Biolabs) or Phusion Polymerase (generated in-house). Plasmids for human ERK1, human ERK2, and TurboID were obtained from Addgene (see key resources table) and subsequently cloned into the d0 backbone. All newly constructed plasmids were sequence-verified by the University of Chicago Comprehensive Cancer Center DNA Sequencing and Genotyping Facility and are available on request.

Western blotting

After SDS–PAGE, proteins were transferred onto methanol-preactivated Immobilon-P PVDF membranes (pore size 0.45 μm; Millipore) using a semi-dry transfer cell or a wet transfer tank (Bio-Rad). After transfer, membranes were treated in accordance with standard Western blotting procedures, using a solution of 3% BSA (ThermoFisher) in TBST (20 mM Tris, pH 7.5, 150 mM NaCl, 0.1% Tween 20) wash buffer. Membranes were visualized using SuperSignal West Pico PLUS chemiluminescent substrate (ThermoFisher) and recorded on a chemiluminescent Western blot imaging system (Azure Biosystems C300). All antibodies used can be found in the key resources table in the STAR Methods section.

Acyl biotin exchange (ABE)

All volumes and reagent amounts are representative for an experiment using a 10 cm plate

Following treatment as required, cells were washed twice with cold DPBS and lysed with 1–2 mL of RIPA lysis buffer (50 mM Tris, 150 mM NaCl, 0.5% deoxycholate, 0.1% SDS, 1.0% Triton X-100, pH 7.4) supplemented with a protease inhibitor cocktail and 50 mM *N*-ethylmaleimide (NEM) (Acros). After end-over-end rotation (4 °C, 3 h), lysates were centrifuged at 13,000*g* (4 °C, 20 min), and the supernatant was collected and subjected to acetone precipitation. The resulting pellet was dissolved by sonication in resuspension buffer (4% SDS, 50 mM HEPES, 150 mM NaCl, 5 mM EDTA, pH 7.4; 100 μL per mg of protein) containing 50 mM NEM. This protein solution was rotated end-over-end (25 °C, 2 h) and then subjected to chloroform–methanol precipitation (2×) to remove excess NEM. The resulting protein pellet was dissolved in 160 μL of resuspension buffer via sonication. The protein sample was divided into two equal parts for ± hydroxylamine (HA) (Combi-Blocks) treatment. Each sample was treated with 320 μL of either -HA Triton buffer (0.2% Triton X-100, 50 mM HEPES, 150 mM NaCl, 5 mM EDTA, pH 7.4) or +HA buffer (Triton buffer +0.7 M HA, pH ~7.2). After shaking incubation (25 °C, 1 h), proteins were precipitated by chloroform–methanol precipitation to remove HA. Protein pellets were resuspended by sonication in 80 μL of resuspension buffer containing 10 μM EZ-Link HPDP-Biotin (ThermoFisher), diluted with 320 μL of Triton buffer containing 10 μM HPDP-Biotin, and incubated with shaking (25 °C, 2 h). Excess biotin was removed with two sequential chloroform-methanol precipitations. Finally, protein pellets were dissolved in 40 μL resuspension buffer via sonication, and the solution volume was brought to 400 μL with Triton buffer. Protein concentration was then measured using the BCA assay (ThermoFisher). Protein (~30–40 μg, 10%) was removed to serve as an expression control ('input'). The remaining solution was diluted with Triton buffer, and streptavidin–agarose beads (50 μL of slurry per 1 mg of protein) were added to each sample, which was then incubated via end-over-end rotation (4 °C, 12 h). Beads were then washed (3 × 1 mL) with wash buffer (Triton buffer +0.1% SDS) to remove unbound protein. Bound proteins ('output') were eluted by boiling the beads (95 °C, 10 min) with 1× Laemelli sample buffer (Alfa Aesar) containing 30 mM DTT. The protein was resolved on 8–12% SDS–PAGE gels and subjected to Western blotting in accordance with the protocol outlined above.

For ABE performed on mouse tissue samples, organs were isolated from C57BL/6J mice, washed with Hanks' balanced salt solution, and flash-frozen in liquid nitrogen. Following mechanical homogenization, samples were lysed in 2–5 mL (depending on organ mass) of HEPES lysis buffer (150 mM NaCl, 40 mM HEPES, 0.5% Triton, 3 mM EDTA, pH 7.4 with protease inhibitors and 1 mM PMSF) containing 50 mM NEM, vortexed vigorously and rotated end-over-end (4°C, 8 h). After centrifugation at 15,000*g*, the supernatant was removed and subjected to sequential acetone and chloroform–methanol precipitations to yield dry protein. The resulting protein pellet was then processed as described above.

To visualize phosphorylated and acylated ERK1/2, phosphatase inhibitor cocktails A and B (see key resources table) were added to the lysis buffer and to subsequent protein solutions throughout the assay.

For ABEs following chemical inhibitor treatment (CMA, PalmB, ML-348, and ML-349), cells were treated at the stated concentrations and times in media containing 0.1% FBS (DMEM, HEK293T cells) or 1% FBS (EMEM, HepG2 cells).

For ABEs following mDHHC library overexpression HEK293T cells first were transfected with HA-tagged mDHHC plasmids (11 μg DNA per 10 cm dish) at 40–60% confluency. At 24 h post transfection, HEK293T cells were washed with DPBS and lysed with 1–2 mL of RIPA lysis buffer (50 mM Tris, 150 mM NaCl, 0.5% deoxycholate, 0.1% SDS, 1.0% Triton X-100, pH 7.4) supplemented with a protease inhibitor cocktail and 50 mM *N*-ethylmaleimide (NEM) (Acros). The resulting lysate was then processed as described above.

For ABEs following APT knockdown in a 10 cm dish, HEK293T cells at 40–60% confluency were transfected with 10 pmol of siRNA targeting either APT1 or APT2, or an NT siRNA control. At 24 h post transfection, HEK293T cells were washed with DPBS and lysed with 1–2 mL of RIPA lysis buffer (50 mM Tris, 150 mM NaCl, 0.5% deoxycholate, 0.1% SDS, 1.0% Triton X-100, pH 7.4) supplemented with a protease inhibitor cocktail and 50 mM *N*-ethylmaleimide (NEM) (Acros). The resulting lysate was then processed as described above.

To quantify changes observed via ABE, each output sample was first normalized to the input protein and then presented as the ratio to the control band.

Metabolic labeling

All volumes and reagent amounts are representative for an experiment using 2 wells of 6 well plate

At 40–60% confluency, HEK293T cells were transfected with HA-tagged mDHHC plasmids (2 μg DNA/well) with or without myc-ERK2(C254A) (0.5 μg DNA/well). At 24 h post transfection, HEK293T cells were washed with DPBS and treated with 50 μM 17-ODYA absorbed on 5% BSA in DMEM GlutaMAX supplemented with 5% charcoal filtered FBS (6 h). Following treatment, cells were washed once in DPBS, lysed with 280 μL HEPES Lysis buffer (150 mM NaCl, 50 mM HEPES, 0.2% SDS, 1% Triton-100, pH 7.4, supplemented with an EDTA-free protease inhibitor cocktail and 1mM PMSF), and subjected to end-over-end rotation (4°C, 12 h).

The cell debris was pelleted by centrifugation at 13000*g* (4°C, 20 min) and the supernatant collected. A master mix (24 μL, per sample, 6 μL each of 5 mM Biotin-Azide, 5 mM TBTA, 50 mM $CuSO_4$ and 5 mM TCEP) was made and added for a 300μL "click" reaction. The resulting solution was incubated (r.t., 1 h) with shaking. 10 μL of 100 mM EDTA was added to quench the "click" reaction and proteins were precipitated by chloroform-methanol precipitation (2×). The resulting protein pellet was dissolved in 40 μL of the resuspension buffer via sonication and the volume was brought to 1600 μL with Triton buffer. Undissolved material was removed by centrifugation at 13,000 g (4°C, 5 min). Two 40 μL protein samples were transferred to fresh tubes ('input' and expression validation). 25 μL of streptavidin-agarose bead slurry was added to 1400 μL of the remaining protein solution, and then samples were incubated with end-over-end rotation (4°C, 12 h). Unbound proteins were removed by washing (6 × 1 mL) with wash buffer. Bound proteins were eluted by boiling the beads (95°C, 10 min) with 1 × Laemelli sample buffer containing 20–30 mM DTT. The protein was resolved on 8–12% SDS-PAGE gels and subjected to Western blotting protocol using the protocol described above.

To quantify changes observed via metabolic labeling, each output sample was first normalized to the input protein and then presented as the ratio to the control band.

Immunoprecipitations

For immunoprecipitation and co-immunoprecipitation experiments, following stated transfections and treatments, cells were lysed in SDS-free RIPA (150 mM Tris, 150 mM NaCl, 0.5% deoxycholate, 1.0% Triton X-100, pH 7.4) supplemented with PMSF and a protease inhibitor cocktail on ice for 10 min, followed by centrifugation at 13,000*g* (4°C, 20 min). Protein concentration was then measured using the BCA assay (ThermoFisher), and protein (20 μg, 'input') was removed and lysate was added to Protein G Dynabeads (Invitrogen: 10003D) pre-incubated with the appropriate antibody. After 12 h of enrichment, beads were washed (3×, SDS-free RIPA) and total protein eluted with 50 mM glycine (pH 2.8) and brought to neutral with 1 μL of 1 M Tris-base, 'output.' Both input and output protein were subjected to separation by SDS-PAGE and Western blotting in accordance with described procedures.

RT-qPCR

For *in cellulo* experiments, HepG2 cells were starved in low-serum media (1% EMEM) for 16 h, and then treated first with DMSO, CMA (20 μM, 3 h), PalmB (20 μM, 3 h), or ML-349 (20 μM, 3 h), and then with EGF (1 ng mL^{-1}) for 0, 30, or 60 min. Total RNA was harvested and isolated using the RNeasy Mini Kit (QIAGEN) and RNA clean & concentration (Zymo). After RNA isolation, RNA was reverse transcribed using the PrimeScript RT Reagent Kit (TaKaRa). All qPCR reactions were run at 20 μL volumes with three biological replicates using PowerUp SYBR Green Master Mix on a QuantStudio 3 Real-Time PCR System (Thermo). Relative expression levels for target genes were calculated using the $2^{-\Delta\Delta}$Ct method, with gene expression first compared to the housekeeping control gene (β2M) cycle threshold (Ct) value and then to the DMSO-treated samples. For mouse experiments, tissue samples were homogenized in Trizol and subjected to phase separation and precipitation to isolate the total RNA. After RNA isolation, RT-qPCR steps were carried out as described above. Relative expression levels for target genes were calculated using the $2^{-\Delta\Delta}$Ct method, with gene expression in DIO mice first compared to the housekeeping control gene (β2M) cycle threshold (Ct) value and then to the DIO-control samples. All qPCR primers can be found in the key resources table, above. Exact p values for statistical analysis reported below.

Target, brain	p value
DHHC3	0.002738
DHHC7	0.013413
DHHC9	0.009586
DHHC14	0.00463
DHHC17	0.002304
DHHC21	0.001567
DHHC23	0.037805
APT1	0.011226
APT2	0.389931

Target, liver	p value
DHHC3	0.241058
DHHC7	0.019486
DHHC9	0.002116
DHHC14	0.000167
DHHC17	0.000598

(*Continued on next page*)

Continued

Target, liver	p value
DHHC21	0.05172
DHHC23	0.18285
APT1	0.012769
APT2	0.000148

TurboID

At 40–60% confluency, HEK293T cells were transfected with ERK2(WT)-TurboID or ERK2(Mutant)-TurboID (10 μg DNA/10 cm dish). At 24 h post transfection, HEK293T cells were starved in 0.1% FBS DMEM media for 12 h. Then the cells were treated with 100 μM Biotin (Sigma) in 0.1% FBS DMEM with or without 1 ng/mL EGF for 12 min. The cells were washed three times with DPBS and lysed in SDS-free RIPA buffer supplemented with PMSF and protease inhibitors on ice for 30 min, followed by centrifuge at 13,000*g* (4°C, 20 min) Protein (20 μg, 'input') was removed and 750 μg lysate was added with streptavidin–agarose beads (30 μL of slurry), which was then incubated via end-over-end rotation (4 °C, 12 h). Beads were then washed (3 × 1 mL) with wash buffer (0.1% SDS, 0.2% Triton X-100, 50 mM HEPES, 150 mM NaCl, 5 mM EDTA, pH 7.4) to remove unbound protein. Bound proteins ('output') were eluted by boiling the beads for 10 min at 95 °C with 1.5 × Laemelli sample buffer (Alfa Aesar) containing 30 mM DTT. The protein was resolved on 8–12% SDS–PAGE gels and subjected to Western blotting in accordance with the protocol outlined above.

QUANTIFICATION AND STATISTICAL ANALYSIS

Statistical analysis was performed using GraphPad Prism 9 (see key resources table). p-values for each experiment was determined as indicated in the figure legends, with values of <0.05 considered significant. The number (n) of replicates or individual data points are described in the figure legends and/or indicated by data points in the figures. Standard deviations (*std*) are indicated with error bars in the figures.